Safeguarding Millimeter Wave Communications Against Randomly Located Eavesdroppers

Ying Ju, Hui-Ming Wang, *Senior Member, IEEE,* Tong-Xing Zheng, *Member, IEEE,* Qinye Yin,
and Moon Ho Lee, *Life Senior Member, IEEE*

Abstract—Millimeter wave offers a sensible solution to the capacity crunch faced by 5G wireless communications. This paper comprehensively studies physical layer security in a multi-input single-output (MISO) millimeter wave system where multiple single-antenna eavesdroppers are randomly located. Concerning the specific propagation characteristics of millimeter wave, we investigate two secure transmission schemes, namely maximum ratio transmitting (MRT) beamforming and artificial noise (AN) beamforming. Specifically, we first derive closed-form expressions of the connection probability for both schemes. We then analyze the secrecy outage probability (SOP) in both non-colluding eavesdroppers and colluding eavesdroppers scenarios. Also, we maximize the secrecy throughput under a SOP constraint, and obtain optimal transmission parameters, especially the power allocation between AN and the information signal for AN beamforming. Numerical results are provided to verify our theoretical analysis. We observe that the density of eavesdroppers, the spatially resolvable paths of the destination and eavesdroppers all contribute to the secrecy performance and the parameter design of millimeter wave systems.

Index Terms—Physical layer security, millimeter wave, multipath, stochastic geometry, artificial noise, secrecy outage, secrecy throughput.

I. INTRODUCTION

Driven by an increasing number of smart devices and wireless data applications, an explosive growth of demand for spectrum in wireless communications appears during the past years. Exploiting millimeter wave becomes a promising approach for providing plentiful spectrum resources to improve the system capacity [1], [2]. Following this trend, the study on millimeter wave communications has attracted great research affords. Millimeter wave channel modeling [3], [4], beamforming schemes [5]-[9] and network performance [10], [11] have been investigated intensively in the past few years. It becomes a promising candidate for the 5G cellular system.

Given the open feature of the wireless channels, security is a significant concern when designing wireless transmission schemes. Physical layer security has become a popular way to improve the secrecy performance of wireless communication systems by utilizing wireless channel characteristics [12]-[14]. Thanks to the application of multi-antenna techniques, physical layer security is greatly enhanced in [15], [16]. With mul-

Y. Ju is with Xi'an Jiaotong University, Xi'an 710049, China, and also with State Radio Monitoring Center, Xi'an 710200, China (e-mail: juyingtju@163.com).

H.-M. Wang, T.-X. Zheng and Q. Yin are with Xi'an Jiaotong University, Xi'an 710049, China (e-mail: xjbswhm@gmail.com; txzheng@stu.xjtu.edu.cn; qyyin@mail.xjtu.edu.cn).

M. H. Lee is with Chonbuk National University, Jeonju 561-756, South Korea (e-mail: moonho@jbnu.ac.kr).

tiple antennas, the transmitter can use transmit beamforming either to enhance the legitimate user's channel, i.e., maximum ratio transmitting (MRT) beamforming [17], or to deteriorate eavesdroppers' channels by emitting artificial noise (AN), i.e., AN beamforming [18], [19]. Also, transmit antenna selection technique can be exploited as an effective approach to improve the quality of the legitimate user's channel [20]. When designing secure transmission schemes, reducing secrecy outage probability (SOP) [17], [20] and increasing secrecy throughput [19] are two significant goals.

In wiretap scenarios, eavesdroppers are always passive and their locations are hard to acquire in practice. To model the unknown locations of potential eavesdroppers, stochastic geometry theory has provided a powerful tool recently, with which eavesdroppers' positions can be represented by a spatial distribution such as a Poisson point process (PPP) [21]-[23]. This makes the secure transmission scheme design and secrecy performance evaluation possible in the wireless systems with potentially unknown eavesdroppers.

We should point out that, the wireless channel significantly influences the design and analysis of physical layer security, and the millimeter wave channel is truly different from the traditional microwave channel which has rich scattering. Based on the measurements conducted in New York City, the ray cluster channel model, constituted by several clusters of propagation paths, is built for millimeter wave systems [4]. This model is further adopted in [5]-[8] to design and analyze millimeter wave beamforming schemes. Therefore, the major concern for the implementation of physical layer security in millimeter wave communication systems is the specific propagation characteristics of millimeter wave, which can be described as follows. Firstly, due to the sparse multipaths and scattering of the millimeter wave propagation environment, traditional statistically independent fading distributions are no longer suitable to model the millimeter wave channel. Channels in the millimeter wave band are correlated fading rather than independent and identically distributed (i.i.d.) Rayleigh. Secondly, the small carrier wavelength of millimeter wave enables the realization of large antenna arrays, which can produce extremely high beamforming gain and directionality [24]. This helps to improve the secrecy performance of millimeter wave transmission [25].

Driven by the new propagation features, studies on secure transmissions in millimeter wave systems spring up, both in point-to-point transmissions [26]-[32] and networks [33]-[35]. Specifically, for the point-to-point millimeter wave systems, switched array techniques are utilized in [26], [27], where

a subset of transmit antennas are randomly selected to emit signals with every symbol period. This results in a clear constellation in the legitimate user's direction and a high symbol error rate in undesired directions. This method that needs only a single RF chain is easy to implement in millimeter wave systems. However, the switching speed to be matched at per-symbol rate leads to a huge system overhead, and the antenna sparsity caused by switching makes the secure transmission vulnerable to attacking [36]. Hybrid beamforming design for millimeter wave systems to resist eavesdropping is studied in [28], [29]. Furthermore, in our previous work [30]-[32], we design beamforming schemes and analyze secrecy performance for the millimeter wave system which contains only one eavesdropper. For the scope of millimeter wave networks, the authors in [33]-[35] analyze the secrecy performance of cellular or Ad hoc networks under the stochastic geometry framework. Both the noise-limited and AN-assisted cellular networks are considered in [33]. The tradeoff between the connection outage probability and secrecy outage probability is investigated for a microwave and millimeter wave hybrid cellular network in [34]. The impact of random blockages and antenna gain on the secrecy performance of Ad hoc networks is analyzed in [35]. These three works focus on the network-wide performance analysis, and the beam pattern is approximated by a sectored antenna model for mathematical tractability.

In all the aforementioned studies, they either do not consider multipath transmission, or do not investigate the effect of multiple randomly distributed eavesdroppers. To the best of our knowledge, no previous work has provided secure transmission schemes and comprehensive secrecy performance analysis under a more practical *ray cluster channel model* that characterizes multipath propagation for a millimeter wave system with the stochastic geometry framework. So far, how to safeguard the point-to-point millimeter wave system against randomly located eavesdroppers under a more practical millimeter wave channel model is still unknown, which motivates our work.

A. Our Work and Contributions

In this paper, we study physical layer security in a multi-input single-output (MISO) millimeter wave system considering multipath propagation under a stochastic geometry framework, where the locations of multiple single-antenna eavesdroppers are modeled as a homogeneous PPP. Connection probability, SOP and secrecy throughput are studied to evaluate the secrecy performance of the transmission schemes. Our contributions are summarized as follows:

1) In the presence of multiple randomly located eavesdroppers, we investigate two transmission schemes, namely MRT beamforming and AN beamforming, under the discrete angular domain channel model which characterized by multiple spatially resolvable paths. We obtain the probability distribution function (PDF) for the number of overlapped common channel paths between the destination and an arbitrary eavesdropper to facilitate the secrecy performance analysis.

2) We derive the closed-form connection probability for both transmission schemes and evaluate the impact of the number of destination's resolvable paths on the connection. Then we obtain the closed-form expressions of SOP for the non-colluding eavesdroppers scenario and the accurate approximation of SOP for the colluding eavesdroppers scenario. In addition, we maximize the secrecy throughput for both schemes, and derive the optimal power allocation between AN and the information signal for the AN scheme. we observe that more power should be allocated to AN in the dense eavesdroppers scenario or in the situation where the number of the destination's resolvable paths or that of the eavesdropper's resolvable paths is large.

3) We reveal that AN beamforming has a better secrecy performance than MRT beamforming when the number of the eavesdropper's resolvable paths is large, the density of eavesdroppers is large or the transmit power is high. Otherwise, MRT beamforming as a simple method shows its superiority. Furthermore, we find that the decrease of the number of the destination's resolvable paths is beneficial for improving the secrecy performance in both beamforming schemes, while the impact of the number of the eavesdropper's resolvable paths on the secrecy throughput are different between two schemes.

B. Organization and Notations

This paper is organized as follows. In Section II, we build the channel model, analyze spatially resolvable paths, and describe performance metrics. In Section III, we propose two secure transmission schemes against randomly located eavesdroppers. In Sections IV and V, we analyze the connection probability, the SOP and the secrecy throughput for both schemes. In Section VI, we provide numerical results to verify our theoretical analysis. In Section VII, we conclude our paper.

We use the following notations in this paper: bold uppercase (lowercase) letters denote matrices (vectors). $(\cdot)^*$, $(\cdot)^T$, $(\cdot)^H$, $|\cdot|$, $\|\cdot\|$, $\mathbb{P}\{\cdot\}$ and $\mathbb{E}_A\{\cdot\}$ denote conjugate, transpose, conjugate transpose, absolute value, Euclidean norm, probability, and mathematical expectation with respect to A, respectively. $\mathcal{CN}(\mu, \sigma^2)$, $\mathrm{Exp}(\lambda)$ and $\mathrm{Gamma}(N, \lambda)$ denote circularly symmetric complex Gaussian distribution with mean μ and variance σ^2, exponential distribution with parameter λ, and gamma distribution with parameters N and λ, respectively. $\mathbb{C}^{M \times N}$ denotes the space of all $M \times N$ matrices with complex-valued elements. $\mathbb{Z}^+$ denotes positive integer domain. $\log(\cdot)$, $\lg(\cdot)$ and $\ln(\cdot)$ denote base-2, base-10 and natural logarithms, respectively. $f_u(\cdot)$, $F_u(\cdot)$ and $F_u^{-1}(\cdot)$ denote the PDF, cumulative distribution function (CDF) of u and inverse function of $F_u(\cdot)$, respectively. The intersection, union and difference between two sets Ω_1 and Ω_2 are denoted by $\Omega_1 \cap \Omega_2$, $\Omega_1 \cup \Omega_2$ and $\Omega_1 \backslash \Omega_2$, respectively. $\mathrm{E}_i(-x) = \int_x^\infty \frac{e^{-t}}{t} dt$ with $x > 0$.

II. SYSTEM MODEL

We consider a millimeter wave system where a transmitter communicates with a destination while randomly located eavesdroppers attempt to intercept the information. The transmitter is equipped with N_t antennas, the destination and

eavesdroppers are all equipped with single antenna[1]. Without loss of generality, we assume the transmitter is located at the origin and the destination is located at coordinate $(r_d, 0)$. As shown in Fig. 1(a), eavesdroppers are located according to a homogeneous PPP Φ_e of density λ on the 2-D plane with the kth eavesdropper having a distance r_k from the transmitter.

A. Discrete Angular Domain Channel Model

Due to the sparse characteristics of the millimeter wave propagation environment, millimeter wave channels can be described by a ray cluster based spatial channel model [4]-[8]. The channel is assumed to be a sum of the contributions of N_c clusters with N_r paths in each cluster and can be formulated as $\mathbf{h} = \sqrt{\frac{\beta}{N_c N_r}} \sum_{l_c} \sum_{l_r} g_{l_c,l_r} \mathbf{a}(\Theta_{l_c,l_r})^H$, where β is the average path loss between the transmitter and the receiver, g_{l_c,l_r} is the complex gain of the l_r^{th} path in the l_c^{th} cluster, $\mathbf{a}(\Theta_{l_c,l_r})$ is the normalized array response at the azimuth angle of departure (AOD) of θ_{l_c,l_r}, and $\Theta_{l_c,l_r} \triangleq \sin(\theta_{l_c,l_r})$. When a uniform linear array (ULA) is adopted, the normalized array response can be described as $\mathbf{a}(\Theta) = \frac{1}{\sqrt{N_t}} \left[1, e^{-j\frac{2\pi d}{\lambda}\Theta}, e^{-j2\frac{2\pi d}{\lambda}\Theta}, \cdots, e^{-j(N_t-1)\frac{2\pi d}{\lambda}\Theta} \right]^T$, where d is the antenna spacing, λ is the wavelength, and generally $d = \frac{\lambda}{2}$.

Based on the ray cluster model, in order to conduct the theoretical analysis of the transmission schemes, the millimeter wave channel is modeled as a discrete angular domain channel model in existing literature [3], [37], [38] and our previous work [30], which can be described as

$$\mathbf{h} = \sqrt{\frac{1}{L}} r^{-\frac{\alpha}{2}} \mathbf{g} \mathbf{U}^H, \tag{1}$$

where $\mathbf{g} = [g_1, g_2, \cdots, g_{Nt}]$ is the complex gain vector, $r^{-\frac{\alpha}{2}}$ is the average path loss, r is the distance between the transmitter and the receiver, $\mathbf{U} \triangleq [\mathbf{a}(\Psi_1), \mathbf{a}(\Psi_2), \cdots, \mathbf{a}(\Psi_{Nt})]$ is the spatially orthogonal basis with $\Psi_i \triangleq \frac{1}{M}(i - 1 - \frac{N_t-1}{2})$ and $M = N_t \frac{d}{\lambda}$. This model is based on the principle that every aperture-limited system has a finite angular resolution [37]. Since paths with Θ differing by less than $\frac{1}{M}$ are not resolvable by the array, the angular domain can be sampled at a fixed spacing $\frac{1}{M}$ and represented by the spatially orthogonal basis $\mathbf{U}$. Experimental results in [4], [39] show that the millimeter wave channel most likely contains only one cluster where the overwhelming proportion of transmit power is concentrated on. Therefore, we assume that signals are transmitted through one cluster and all the AODs of paths are distributed within the angular range $[\theta_{\min}, \theta_{\max}]$. If $\Psi_i \in [\sin(\theta_{\min}), \sin(\theta_{\max})]$, the ith column of $\mathbf{U}$ (the ith orthogonal basis vector) represents a spatially resolvable path and we assume that the ith complex gain g_i is a complex Gaussian coefficient with $g_i \sim \mathcal{CN}(0, 1)$; otherwise, $g_i = 0$ [4], [24], [30]. L is defined as the number of spatially resolvable paths with $L < N_t$. Then the channels of the destination and the kth eavesdropper can be described

[1]This assumption is used for tractability. In practice, multiple receive antennas are equipped and they will form a receive beam, which is equivalent to a directional single antenna. This will not influence the analysis performed in this paper. Similar assumption has also been adopted by [5], [26], [27], [29]-[34], etc.
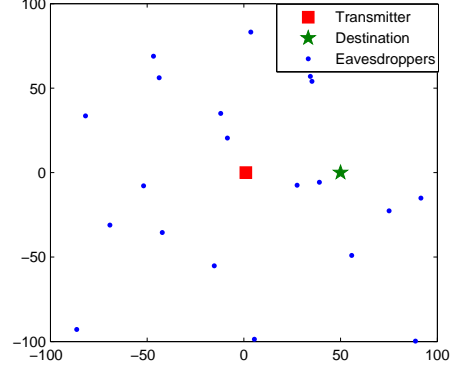
(a) Locations of randomly distributed eavesdroppers
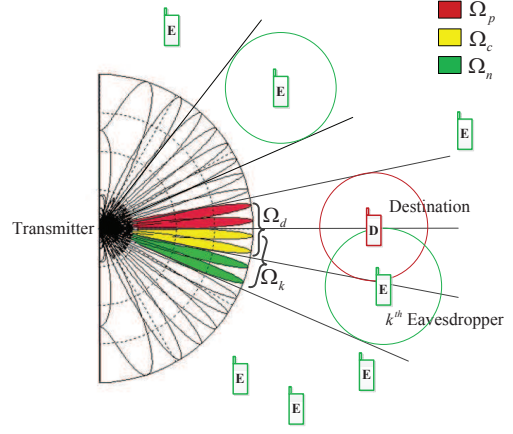
(b) Description of spatially resolvable paths

Fig. 1. Millimeter wave system model with stochastic geometry framework.

as $\mathbf{h}_d = \sqrt{\frac{1}{L_d}} r_d^{-\frac{\alpha}{2}} \mathbf{g}_d \mathbf{U}^H$ and $\mathbf{h}_k = \sqrt{\frac{1}{L_e}} r_k^{-\frac{\alpha}{2}} \mathbf{g}_k \mathbf{U}^H$, where L_d and L_e are the numbers of the destination's and each eavesdropper's resolvable paths, respectively.

We assume the AODs of all the destination's paths and those of the kth eavesdropper's paths are distributed within the angular range $[\theta_{d,\min}, \theta_{d,\max}]$ and $[\theta_{k,\min}, \theta_{k,\max}]$ respectively. As shown in Fig. 1(b), we define the set $\Omega_d \triangleq \{I_{d,i} | I_{d,i} \in \mathbb{Z}^+, \Psi_{I_{d,i}} \in [\sin(\theta_{d,\min}), \sin(\theta_{d,\max})], I_{d,1} < I_{d,2} < \cdots < I_{d,L_d}\}$, where $I_{d,i}$ is an index of the orthogonal basis vector which represents a destination's spatially resolvable path. Define the set $\Omega_k \triangleq \{I_{k,i} | I_{k,i} \in \mathbb{Z}^+, \Psi_{I_{k,i}} \in [\sin(\theta_{k,\min}), \sin(\theta_{k,\max})], I_{k,1} < I_{k,2} < \cdots < I_{k,L_e}\}$, where $I_{k,i}$ is an index of the orthogonal basis vector which represents a resolvable path of the kth eavesdropper. Define $\Omega = \{1, 2, \cdots, N_t\}$, $\Omega_a \triangleq \overline{\Omega}_d = \Omega \backslash \Omega_d$, $\Omega_{c,k} \triangleq \Omega_d \cap \Omega_k$ and $\Omega_{p,k} \triangleq \Omega_d \backslash \Omega_{c,k}$, $\Omega_{n,k} \triangleq \Omega_k \backslash \Omega_{c,k}$. Also, we denote $L_{c,k}$ as the number of the overlapped common paths between the destination and the kth eavesdropper. For notational brevity, we omit k from $L_{c,k}$, $\Omega_{c,k}$, $\Omega_{p,k}$ and $\Omega_{n,k}$, and treat L_c, Ω_c, Ω_p and Ω_n as functions of k by default. We define the function $\mathcal{S}(\mathbf{B}, \Omega_s)$ to generate a matrix whose columns are selected from $\mathbf{B}$, and Ω_s contains all the selected columns' indexes. Define $\mathbf{g}_{\varrho\nu} \triangleq \mathcal{S}(\mathbf{g}_\varrho, \Omega_\nu) \in \mathbb{C}^{1 \times L_\nu}$, where $\varrho \in \{d, k\}$, $\nu \in \{c, p, n, a\}$, and L_ν is the cardinality of Ω_ν.

We assume that the instantaneous channel state information

(CSI) of the destination is perfectly known at the transmitter [18], [19]. Since eavesdroppers passively receive signals, their instantaneous CSIs are unknown, whereas the distribution of $\mathbf{g}_k$ is available.

B. Spatially Resolvable Paths

Unlike the traditional wireless channels with rich scattering, the millimeter wave channel involves a limited angular coverage which is represented by the directions of propagation paths. As we have demonstrated in [30], the secrecy performance of the millimeter wave system is dramatically influenced by L_c, which is the number of the overlapped common paths between the eavesdropper's and the destination's spatially resolvable paths. When L_c becomes larger, the correlation between the channel of the destination and that of the eavesdropper is larger. More confidential information is leaked to the eavesdropper so that the secrecy performance will be poorer. However, under the stochastic geometry framework, it is hard to get the exact value of L_c due to the randomness of eavesdroppers' locations and the lack of eavesdroppers' CSIs. Fortunately, we derive the PDF of L_c in the following lemma, which will be extensively used in subsequent sections.

Lemma 1: The PDF of L_c can be given by

$$p(L_c) = \begin{cases} \dfrac{\sum_{i=L_l}^{L_u} \omega_i}{\pi}, & L_c = L_l, \\[2mm] \dfrac{2\omega_{L_c}}{\pi}, & L_c = 1, 2, \cdots, L_l - 1, \\[2mm] 1 - \sum_{i=1}^{L_l} p(i), & L_c = 0, \end{cases} \quad (2)$$

where $\omega_i \triangleq \arcsin\left(\Psi_{\frac{N_t - L_d}{2} + i + 1}\right) - \arcsin\left(\Psi_{\frac{N_t - L_d}{2} + i}\right)$, $L_l \triangleq \min\{L_d, L_e\}$ and $L_u \triangleq \max\{L_d, L_e\}$.

Proof 1: Eavesdroppers are located according to a homogeneous PPP so that the angles of eavesdroppers' locations are uniformly distributed within the range $[-\frac{\pi}{2}, \frac{\pi}{2}]$. In order to get the probability of $L_c = m$, $m \in \{0, 1, \cdots, \min\{L_d, L_e\}\}$, we need to know the angular range Υ_m which satisfies that, the destination and the kth eavesdropper will have m overlapped common resolvable paths when the kth eavesdropper is located in Υ_m. In other words, $[\theta_{k,\min}, \theta_{k,\max}]$ should cover m destination's spatially resolvable paths, where $[\theta_{k,\min}, \theta_{k,\max}]$ is the angular range where AODs of the kth eavesdropper' paths are distributed in as discussed in the last subsection. Then we can obtain the probability $p(m) = \frac{\mathcal{W}(\Upsilon_m)}{\pi}$, where $\mathcal{W}(\cdot)$ denotes the width of an angular range. With this idea in mind, we move the kth eavesdropper to find out the angular range Υ_m as shown in Fig. 2.

Since the destination is located at $(r_d, 0)$ and with L_d resolvable paths, we have $\Omega_d = \{\frac{N_t - L_d}{2} + 1, \frac{N_t - L_d}{2} + 2, \cdots, \frac{N_t + L_d}{2} - 1, \frac{N_t + L_d}{2}\}$ where $\Omega_{d,i} = \frac{N_t - L_d}{2} + i$. Define the angular range $\Delta_i \triangleq \left[\arcsin\left(\Psi_{\frac{N_t - L_d}{2} + i}\right), \arcsin\left(\Psi_{\frac{N_t - L_d}{2} + i + 1}\right)\right]$, and the width $\omega_i \triangleq \mathcal{W}(\Delta_i) = \arcsin\left(\Psi_{\frac{N_t - L_d}{2} + i + 1}\right) - \arcsin\left(\Psi_{\frac{N_t - L_d}{2} + i}\right)$. We find that Δ_i describes the angular range between the ith and the $(i+1)^{th}$ spatially resolvable paths of the destination

(a) $L_c = 1$

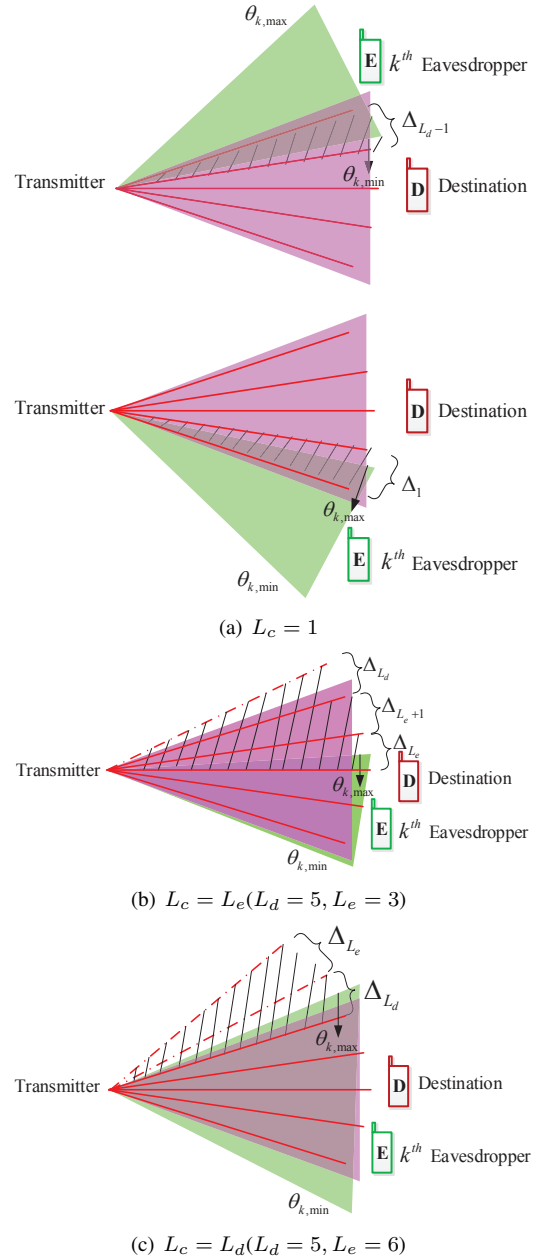(b) $L_c = L_e (L_d = 5, L_e = 3)$

(c) $L_c = L_d (L_d = 5, L_e = 6)$

Fig. 2. Distribution for the number of the overlapped common paths between the destination and the kth eavesdropper. The pink area shows the angular range $[\theta_{d,\min}, \theta_{d,\max}]$ where AODs of the destination's paths are distributed in, and the green area shows the angular range $[\theta_{k,\min}, \theta_{k,\max}]$ where AODs of the kth eavesdropper's paths are distributed in. Red solid lines are the spatially resolvable paths of the destination. Each red dashed line represents an angle in $\mathbf{U}$ but not the spatially resolvable path of the destination. (a) describes the situation that $L_c = 1$, which is similar as all the situations when $L_c < L_l$. (b) and (c) describe the situation that $L_c = L_l$ with $L_d > L_e$ and $L_d < L_e$ respectively.

when $1 \leq i \leq L_d - 1$. Due to the symmetry of the sine function and the definition of Ψ_i, we have $\omega_i = \omega_{L_d-i}$.

As shown in Fig. 2(a), if $\theta_{k,\max}$ is located within Δ_1 or $\theta_{k,\min}$ is located within Δ_{L_d-1}, we have $L_c = 1$. Thus we derive the PDF of $L_c = 1$, which is $p(1) = \frac{\omega_1 + \omega_{(L_d-1)}}{\pi} = \frac{2\omega_1}{\pi}$. Then we analyze two different cases $L_d \geq L_e$ and $L_d < L_e$.

1) $L_d \geq L_e$

In this case, $0 \leq L_c \leq L_e$. From the analysis of $L_c = 1$ given above, we derive the PDFs $p(L_c) = \frac{2\omega_{L_c}}{\pi}, L_c = 1, 2, \cdots, L_e - 1$ by analogy. The situation when $L_c = L_e$ is special. As shown in Fig. 2(b), when $\theta_{k,\max} \in \Delta_{L_e} \cup \Delta_{L_e+1} \cup \cdots \cup \Delta_{L_d}, L_c = L_e$, hence we have $p(L_c) = \frac{\sum_{i=L_e}^{L_d} \omega_i}{\pi}$.

2) $L_d < L_e$

In this case, $0 \leq L_c \leq L_d$, and we derive the PDFs $p(L_c) = \frac{2\omega_{L_c}}{\pi}, L_c = 1, 2, \cdots, L_d - 1$. As shown in Fig. 2(c), when $\theta_{k,\max} \in \Delta_{L_d} \cup \Delta_{L_d+1} \cup \cdots \cup \Delta_{L_e}, L_c = L_d$, hence we have $p(L_c) = \frac{\sum_{i=L_d}^{L_e} \omega_i}{\pi}$.

Combining the above two cases completes the proof.

C. Wiretap Encoding Scheme and Performance Metrics

We consider both non-colluding eavesdroppers and colluding eavesdroppers scenarios. In non-colluding eavesdroppers scenario, each eavesdropper individually decodes confidential messages and the equivalent signal-to-interference-plus-noise ratio (SINR) of the wiretap channel can be expressed as $\xi_e = \max_{e_k \in \Phi_e} \xi_k$, where ξ_k is the received SINR of the kth eavesdropper. In colluding eavesdropper scenario, eavesdroppers jointly decode confidential messages with maximum ratio combining reception and $\xi_e = \sum_{e_k \in \Phi_e} \xi_k$. Then the capacities of the destination's channel and the wiretap channel are $C_d = \log(1 + \xi_d)$ and $C_e = \log(1 + \xi_e)$. Adopting the well-known Wyner's wiretap encoding scheme, we denote the codeword rate and secrecy rate as R_t and R_s. In addition, we define $R_e \triangleq R_t - R_s$ as the rate redundancy to resist the interception. We analyze the following metrics to evaluate the secrecy performance of transmission schemes.

Connection probability: Only if $C_d > R_t$, the destination is able to decode the confidential message correctly. This corresponds to a reliable connection event. We define connection probability as

$$\mathcal{P}_c = \mathbb{P}\{C_d > R_t\}. \tag{3}$$

Secrecy outage probability: If $C_e > R_e$, perfect secrecy is broken and a secrecy outage occurs. We adopt an on-off transmission scheme proposed in [19], where the transmitter decides whether to transmit or not based on the instantaneous CSI of the destination. Throughout the paper, for notational brevity, we define $\mu \triangleq \|\mathbf{g}_d\|^2$ as the overall channel gain of the destination and δ as the transmission threshold. Since the channel gain μ varies from time to time, the transmitter emits signals only when $\mu > \delta$; otherwise, the transmission suspends. The SOP is defined as

$$\mathcal{P}_{so} = \mathbb{P}\{C_e > R_t - R_s | \mu\}, \ \forall \mu > \delta. \tag{4}$$

Secrecy throughput: Secrecy throughput is defined as the effective average transmission rate of the confidential message, which is formulated as

$$\tau = \mathbb{E}_\mu \left[R_s(\mu) \right], \tag{5}$$

where $R_s(\mu) = 0$ for $\mu \leq \delta$.

III. TRANSMISSION SCHEMES

In this section, we propose two transmission schemes, namely MRT beamforming and AN beamforming, to resist overhearing of multiple randomly located eavesdroppers.

A. MRT Beamforming

By exploiting MRT beamforming, the signals received at the destination and the kth eavesdropper are $y_d^{MRT} = \sqrt{P}\mathbf{h}_d\mathbf{w}_1 s + n_d$ and $y_k^{MRT} = \sqrt{P}\mathbf{h}_k\mathbf{w}_1 s + n_k$, where $\mathbf{w}_1 = \mathbf{h}_d^H / \|\mathbf{h}_d\|$ is the beamforming vector, P is the total transmit power, s is the information bearing signal with $\mathbb{E}[|s|^2] = 1$, n_d and n_k are i.i.d. additive white Gaussian noise with $n_d \sim \mathcal{CN}(0, \sigma_n^2)$ and $n_k \sim \mathcal{CN}(0, \sigma_n^2)$. We define $\mu_{c,k} \triangleq \|\mathbf{g}_{dc}\|^2$ and $\mu_{p,k} \triangleq \|\mathbf{g}_{dp}\|^2$ as the destination's channel gain of the common paths and the non-common paths with the kth eavesdropper. For notational brevity, we omit k from $\mu_{c,k}$ and $\mu_{p,k}$, and treat them as functions of k by default. We easily find that $\mu = \mu_c + \mu_p$. Then the SNRs of the destination and the kth eavesdropper can be respectively described as

$$\xi_d^{MRT} = \frac{Pr_d^{-\alpha}}{\sigma_n^2 L_d} \|\mathbf{g}_d\mathbf{U}^H\|^2 = c\mu r_d^{-\alpha}, \tag{6}$$

$$\xi_k^{MRT} = \frac{Pr_k^{-\alpha}|\mathbf{g}_k\mathbf{U}^H\mathbf{U}\mathbf{g}_d^H|^2}{\sigma_n^2 L_e \|\mathbf{g}_d\mathbf{U}^H\|^2} = \frac{a\mu_c r_k^{-\alpha}|\mathbf{g}_{kc}\frac{\mathbf{g}_{dc}^H}{\|\mathbf{g}_{dc}\|}|^2}{\mu}. \tag{7}$$

where $a \triangleq \frac{P}{L_e \sigma_n^2}$ and $c \triangleq \frac{P}{L_d \sigma_n^2}$. We find that $g_{k,i}g_{d,i}^* \neq 0$ only if $i \in \Omega_d \cap \Omega_k$, i.e., $i \in \Omega_c$. Thus we have $\mathbf{g}_k\mathbf{g}_d^H = \mathbf{g}_{kc}\mathbf{g}_{dc}^H$.

B. AN Beamforming

Based on the CSI of the destination, we design the AN beamforming matrix as $\mathbf{W}_2 = \mathcal{S}(\mathbf{U}, \Omega_a)$ to transmit AN to the null space of the destination's channel. Since $\Omega_a = \Omega \backslash \Omega_d$, we have $\mathbf{h}_d\mathbf{W}_2 = \mathbf{0}$, hence the destination is not influenced by AN. We observe that by leveraging the specific propagation characteristics of millimeter wave, we form the null space only through selecting some columns from $\mathbf{U}$, which is really simple to operate. Then signals received by the destination and the kth eavesdropper can be described as $y_d^{AN} = \sqrt{\eta P}\mathbf{h}_d\mathbf{w}_1 s + \sqrt{\frac{(1-\eta)P}{N_t-L_d}}\mathbf{h}_d\mathbf{W}_2\mathbf{z} + n_d$ and $y_k^{AN} = \sqrt{\eta P}\mathbf{h}_k\mathbf{w}_1 s + \sqrt{\frac{(1-\eta)P}{N_t-L_d}}\mathbf{h}_k\mathbf{W}_2\mathbf{z} + n_k$, where $\mathbf{z} \in \mathbb{C}^{(N_t-L_d)\times 1}$ is the AN bearing signal with $\mathbb{E}[\mathbf{z}\mathbf{z}^H] = \mathbf{I}_{N_t-L_d}$, η is the power allocation ratio of the information signal power to the total transmit power with $0 \leq \eta \leq 1$. When $\eta = 1$, AN beamforming is equivalent to MRT beamforming where information signal is transmitted with full power. The SINRs

of the destination and the kth eavesdropper can be respectively formulated as

$$\xi_d^{AN} = \frac{\eta P r_d^{-\alpha}}{\sigma_n^2 L_d} \|\mathbf{g}_d \mathbf{U}^H\|^2 = \eta c \mu r_d^{-\alpha}, \tag{8}$$

$$\xi_k^{AN} = \frac{\frac{\eta P r_k^{-\alpha}}{L_e \mu}|\mathbf{g}_k \mathbf{U}^H \mathbf{U}\mathbf{g}_d^H|^2}{\frac{(1-\eta)P r_k^{-\alpha}}{(N_t - L_d)L_e}\|\mathbf{g}_k \mathbf{U}^H \mathbf{W}_2\|^2 + \sigma_n^2}$$

$$= \frac{\frac{\eta a \mu_c r_k^{-\alpha}}{\mu}|\mathbf{g}_{kc}\frac{\mathbf{g}_{dc}^H}{\|\mathbf{g}_{dc}\|}|^2}{\frac{(1-\eta)a r_k^{-\alpha}}{(N_t - L_d)}\|\mathbf{g}_{kn}\|^2 + 1}. \tag{9}$$

By denoting $\mathbf{g}_k \mathbf{U}^H \mathbf{W}_2 = [\chi_1, \chi_2, \cdots, \chi_{(N_t - L_d)}]$, we have $\chi_j = \sum_{i=1}^{N_t} g_{k,i}\mathbf{a}(\Psi_i)^H \mathbf{w}_{2,j}$. Since $\mathbf{W}_2 = \mathcal{S}(\mathbf{U}, \Omega_a)$ and $\mathbf{U}$ is a unitary matrix, we get $\mathbf{g}_k \mathbf{U}^H \mathbf{W}_2 = \mathbf{g}_{ka}$. Since $\Omega_n = \Omega_k \backslash \Omega_c$, by getting rid of those zero elements in $\mathbf{g}_{ka}$, we have $\|\mathbf{g}_{ka}\| = \|\mathbf{g}_{kn}\|$.

IV. SECRECY PERFORMANCE OF MRT BEAMFORMING

In this section, we analyze the secrecy performance in terms of the connection probability, the SOP and the secrecy throughput for MRT beamforming.

A. Connection Probability

Since $\mu \sim \text{Gamma}(L_d, 1)$, connection probability of MRT beamforming defined in (3) can be described as

$$\mathcal{P}_c = \mathbb{P}\{C_d > R_t\} = \mathbb{P}\{\xi_d^{MRT} > 2^{R_t} - 1\}$$
$$= \frac{1}{\Gamma(L_d)}\Gamma\left(L_d, \frac{(2^{R_t} - 1)r_d^{\alpha}}{c}\right), \tag{10}$$

where $\Gamma(\cdot)$ is the gamma function, and $\Gamma(\cdot, \cdot)$ denotes the upper incomplete gamma function with $\Gamma(n, x) = (n - 1)! \, e^{-x} \sum_{m=0}^{n-1} \frac{x^m}{m!}$.

B. Secrecy Outage Performance

1) Non-Colluding Eavesdroppers: We first derive the CDF of ξ_k^{MRT} in (7). Define $u \triangleq \left|\mathbf{g}_{kc}\frac{\mathbf{g}_{dc}^H}{\|\mathbf{g}_{dc}\|}\right|^2$, Since each element of $\mathbf{g}_{kc}$ follows a Gaussian distribution with zero mean and unit variance, which is independent of the unit-norm vector $\frac{\mathbf{g}_{dc}^H}{\|\mathbf{g}_{dc}\|}$, we have $u \sim \text{Exp}(1)$. The CDF of ξ_k^{MRT} is given by

$$F_{\xi_k}(x) = \mathbb{P}\left\{\frac{a\mu_c r_k^{-\alpha}}{\mu} u < x\right\} = 1 - e^{-\frac{\mu x r_k^{\alpha}}{a\mu_c}}. \tag{11}$$

From the definition of μ_c, we find that $\mu_c \sim \text{Gamma}(L_c, 1)$. Then the CDF of ξ_e can be calculated as

$$F_{\xi_e}(x) = \mathbb{P}\left\{\max_{e_k \in \Phi_e} \xi_k < x\right\} = \mathbb{E}_{\Phi_e, \{\mu_c\}}\left[\prod_{e_k \in \Phi_e}\mathbb{P}\{\xi_k < x\}\right]$$

$$\overset{(a)}{=} \exp\left\{-\lambda \int_0^{\infty}\int_0^{2\pi}\mathbb{E}_{\mu_c}\left\{e^{-\frac{\mu x r_k^{\alpha}}{a\mu_c}}\right\} r_k d\theta dr_k\right\}$$

$$= \exp\left\{-\pi\lambda\Gamma\left(\frac{2}{\alpha} + 1\right)\left(\frac{\mu x}{a}\right)^{-\frac{2}{\alpha}}\sum_{L_c=1}^{L_l}p(L_c)\right.$$

$$\left.\times \mathbb{E}_{\mu_c}\left\{\left(\frac{1}{\mu_c}\right)^{-\frac{2}{\alpha}}\right\}\right\}$$

$$= \exp\left\{-\pi\lambda\Gamma\left(\frac{2}{\alpha} + 1\right)\left(\frac{\mu x}{a}\right)^{-\frac{2}{\alpha}}\sum_{L_c=1}^{L_l}p(L_c)\frac{\Gamma(L_c + \frac{2}{\alpha})}{\Gamma(L_c)}\right\}, \tag{12}$$

where (a) holds for the probability generating functional lemma (PGFL) over PPP [41]. We need to mention that when $L_c = 0$, $\mathbf{g}_{kc}$ and $\mathbf{g}_{dc}^H$ in (7) both equal to 0, hence we have $\xi_k = 0$ and $\mathbb{P}\{\xi_k < x\} = 1$. Since the formula $\prod_{e_k \in \Phi_e}\mathbb{P}\{\xi_k < x\}$ is a multiplication operation, the case $L_c = 0$ does not contribute to F_{ξ_e}. Therefore, we only consider L_c from 1 to L_l.

With the CDF of ξ_e, we obtain the SOP defined in (4) as

$$\mathcal{P}_{so}(\mu) = \mathbb{P}\{C_e > C_d - R_s|\mu\}$$

$$= \mathbb{P}\left\{\xi_e^{MRT} > \frac{\xi_d^{MRT} - (T - 1)}{T}\right\}$$

$$= 1 - \exp\left\{-\pi\lambda\Gamma\left(\frac{2}{\alpha} + 1\right)\left(\frac{\mu[c\mu r_d^{-\alpha} - (T - 1)]}{aT}\right)^{-\frac{2}{\alpha}}\right.$$

$$\left.\times \sum_{L_c=1}^{L_l}p(L_c)\frac{\Gamma(L_c + \frac{2}{\alpha})}{\Gamma(L_c)}\right\}. \tag{13}$$

where $T \triangleq 2^{R_s}$.

2) Colluding Eavesdroppers: In this scenario, secrecy outage probability can be written by $\mathcal{P}_{so}(\mu) = \mathbb{P}\left\{\frac{a}{\mu}\sum_{e_k \in \Phi_e}\mu_c u r_k^{-\alpha} > \frac{c\mu r_d^{-\alpha} - (T-1)}{T}\right\} = \mathbb{P}\left\{I_e > \frac{\mu[c\mu r_d^{-\alpha} - (T-1)]}{aT}\right\}$, where $I_e \triangleq \sum_{e_k \in \Phi_e}\mu_c u r_k^{-\alpha}$. We first calculate the Laplace transform of I_e by

$$\mathcal{L}_{I_e}(s) = \mathbb{E}_{\Phi_e, u, \mu_c}\left[e^{-s\sum_{e_k \in \Phi_e}\mu_c u r_k^{-\alpha}}\right]$$

$$= \mathbb{E}_{\Phi_e}\left\{\prod_{e_k \in \Phi_e}\mathbb{E}_{u, \mu_c}\left[\exp\left(-s\mu_c u r_k^{-\alpha}\right)\right]\right\}$$

$$\overset{(b)}{=} \exp\left\{-\lambda\sum_{L_c=1}^{L_l}2\pi p(L_c)\mathbb{E}_{u, \mu_c}\right.$$

$$\left.\times\left[\int_0^{\infty}\left[1 - \exp\left(-s\mu_c u r_k^{-\alpha}\right)\right]r_k dr_k\right]\right\}$$

$$= \exp\left\{-\pi\lambda\sum_{L_c=1}^{L_l}p(L_c)s^{\frac{2}{\alpha}}\Gamma(1 - \frac{2}{\alpha})\mathbb{E}_u\left(u^{\frac{2}{\alpha}}\right)\mathbb{E}_{\mu_c}\left(\mu_c^{\frac{2}{\alpha}}\right)\right\}$$

$$= \exp\left\{-\pi\lambda s^{\frac{2}{\alpha}}\Gamma(1 - \frac{2}{\alpha})\Gamma(1 + \frac{2}{\alpha})\sum_{L_c=1}^{L_l}p(L_c)\frac{\Gamma(L_c + \frac{2}{\alpha})}{\Gamma(L_c)}\right\}, \tag{14}$$

where (b) holds for PGFL over PPP.

After deriving $\mathcal{L}_{I_e}(s)$, we can obtain the CDF of I_e through inverse Laplace transform, and then get the SOP. However, inverse Laplace transform causes considerable calculation complexity and induces analysis intractable. Therefore, we provide an approximation of $\mathcal{P}_{so}$ in the following theorem.

Theorem 1: The SOP in the scenario of colluding eavesdroppers for MRT beamforming can be approximated as

$$\mathcal{P}_{so} \gtrapprox \sum_{n=0}^{N}\binom{N}{n}(-1)^n \mathcal{L}_{I_e}\left(\frac{qaTn}{\mu[c\mu r_d^{-\alpha} - (T-1)]}\right), \tag{15}$$

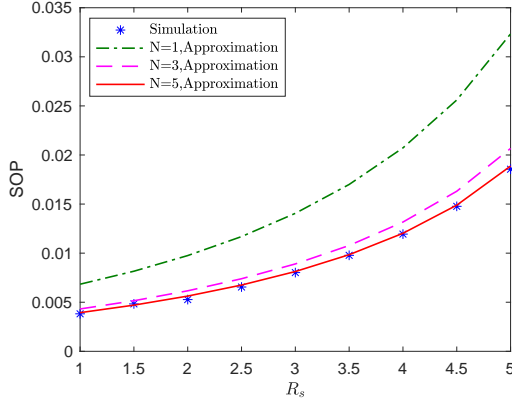Fig. 3. SOP versus R_s for different N's, with $N_t = 100$, $P = 0$dBm, $r_d = 50$m, $L_d = 20$, $L_e = 20$, $\alpha = 4$ and $\lambda = 10^{-5}$.

where $\mathcal{L}_{I_e}(s)$ is given by (14), $q \triangleq N(N!)^{-\frac{1}{N}}$ and N is defined as the number of terms used in approximation.

Proof 2: Defining ι as a normalized gamma random variable with the shape parameter N, we have

$$
\begin{aligned}
\mathcal{P}_{so}(\mu) &= \mathbb{P}\left\{\frac{aTI_e}{\mu[c\mu r_d^{-\alpha} - (T-1)]} > 1\right\} \\
&\overset{(c)}{\approx} \mathbb{P}\left\{\frac{aTI_e}{\mu[c\mu r_d^{-\alpha} - (T-1)]} > \iota\right\} \\
&\overset{(d)}{\gtrapprox} \left\{1 - \exp\left[-\frac{qaTI_e}{\mu[c\mu r_d^{-\alpha} - (T-1)]}\right]\right\}^N,
\end{aligned}
\tag{16}
$$

where (c) holds for the fact that a normalized gamma random variable converges to identity when its shape parameter goes to infinity, and (d) follows the CDF bound of a normalized gamma random variable [10], [33]. By using binomial expansion, we obtain the tight lower bound of $\mathcal{P}_{so}$ given in (15).

As shown in Fig. 3, $\mathcal{P}_{so}$ given in Theorem 1 is more similar to the simulation results when N becomes larger, and we get a good approximation when N increases to 5. Thus we use $N = 5$ in the following numerical analysis. In addition, we find that $\mathcal{P}_{so}$ increases when R_s increases. The underlying reason is that when we set a higher R_s, the rate redundancy $R_e = R_t - R_s$ which is utilized to against the eavesdropping becomes lower and the secrecy outage requirement $C_e > R_e$ is easier to meet.

C. Secrecy Throughput Maximization

In this subsection, we maximize the secrecy throughput subject to a tolerable SOP constraint in the non-colluding eavesdroppers scenario. We first maximize $R_s(\mu)$ and formulate the optimization problem as

$$
\max_{R_t, \delta} \ R_s(\mu),
$$

$$
s.t. \quad 0 < R_s(\mu) < R_t \le C_d, \tag{17a}
$$

$$
\mathcal{P}_{so}(\mu) \le \epsilon, \tag{17b}
$$

where $\epsilon \in [0, 1]$ is the SOP threshold. Following the definition formula of the SOP in (4), the SOP constraint can be rewritten as $\mathcal{P}_{so}(\mu) = 1 - F_{\xi_e}(2^{R_t - R_s} - 1) \le \epsilon$. Since

$F_{\xi_e}(x)$ is a monotonically increasing function, we obtain $R_s \le R_t - \log(1 + F_{\xi_e}^{-1}(1 - \epsilon))$, where $F_{\xi_e}^{-1}(\cdot)$ denotes the inverse function of $F_{\xi_e}(\cdot)$. As R_t should not exceed C_d, we set R_t equal to C_d to achieve a maximum R_s, which is

$$
R_s^*(\mu) = [C_d - \log(1 + F_{\xi_e}^{-1}(1 - \epsilon))]^+. \tag{18}
$$

From (12), by denoting $\rho \triangleq F_{\xi_e}^{-1}(1 - \epsilon)$, we have $\rho = \frac{a\varpi}{\mu}$ with $\varpi \triangleq \left[-\frac{\pi\lambda\Gamma\left(\frac{2}{\alpha}+1\right)}{\ln(1-\epsilon)}\sum_{L_c=1}^{L_l} p(L_c)\frac{\Gamma(L_c + \frac{2}{\alpha})}{\Gamma(L_c)}\right]^{\frac{\alpha}{2}}$. In addition, in order to obtain a positive R_s^*, $C_d > \log(1 + \rho)$ should be satisfied. Since $C_d = \log(1 + c\mu r_d^{-\alpha})$, the maximum $R_s(\mu)$ of MRT beamforming can be given by

$$
R_s^*(\mu) = \log\frac{1 + c\mu r_d^{-\alpha}}{1 + \rho}, \tag{19}
$$

with the transmission constraint $\mu > \delta = \sqrt{\frac{z_1 r_d^\alpha}{c}}$, where $z_1 \triangleq \varpi a = \rho\mu$, and δ is the transmission threshold. According to the on-off transmission scheme, the transmitter radiates signals with $R_s^*(\mu)$ only when $\mu > \delta$; otherwise, the transmitter keeps silence and we set $R_s(\mu) = 0$. After obtaining $R_s^*(\mu)$, we calculate the maximum secrecy throughput according to (5).

Theorem 2: The maximum secrecy throughput of MRT beamforming can be given by

$$
\tau^* = \sum_{m=0}^{L_d-1} \frac{e^{-\delta}\delta^{L_d-1-m}}{\Gamma(L_d - m)}\left[V\left(\frac{1}{\delta}\right) + V\left(\frac{cr_d^{-\alpha}}{1 + cr_d^{-\alpha}\delta}\right) \right.
$$
$$
\left. -V\left(\frac{1}{\delta + z_1}\right) + \log\frac{\delta(1 + cr_d^{-\alpha}\delta)}{\delta + z_1}\right], \tag{20}
$$

where $V(x) = \frac{1}{\ln 2}\sum_{n=1}^{m}\frac{1}{(m-n)!}\left[\frac{(-1)^{m-n-1}}{x^{m-n}}e^{\frac{1}{x}}\text{Ei}\left(-\frac{1}{x}\right) + \sum_{k=1}^{m-n}(k-1)!\left(-\frac{1}{x}\right)^{m-n-k}\right]$.

Proof 3: Please see Appendix A.

Corollary 1: τ^* monotonically decreases with r_d and λ, while monotonically increases with ϵ.

Proof 4: From $\tau^* = \int_\delta^\infty R_s^*(x)f_\mu(x)dx = \int_\delta^\infty \log\frac{1 + cxr_d^{-\alpha}}{1 + \frac{z_1}{x}}f_\mu(x)dx$, we have $\frac{\partial\tau^*}{\partial\delta} < 0$, $\frac{\partial\tau^*}{\partial z_1} < 0$ and $\frac{\partial\tau^*}{\partial r_d} < 0$, hence we derive $\frac{d\tau^*}{dz_1} = \frac{\partial\tau^*}{\partial\delta}\frac{d\delta}{dz_1} + \frac{\partial\tau^*}{\partial z_1} < 0$. Therefore, we obtain $\frac{d\tau^*}{d\lambda} = \frac{d\tau^*}{dz_1}\frac{dz_1}{d\lambda} < 0$, $\frac{d\tau^*}{d\epsilon} = \frac{d\tau^*}{dz_1}\frac{dz_1}{d\epsilon} > 0$ and $\frac{d\tau^*}{dr_d} = \frac{\partial\tau^*}{\partial\delta}\frac{d\delta}{dr_d} + \frac{\partial\tau^*}{\partial r_d} < 0$.

Corollary 1 implies that MRT beamforming achieves higher secrecy throughput in a sparser eavesdroppers scenario, under a more moderate SOP constraint, or when the distance between the destination and the transmitter is smaller.

Corollary 2: At the high transmit power regime, i.e., $P \to \infty$, The maximum secrecy throughput of MRT beamforming is given in (21), and is independent of P.

$$
\tau^* = \sum_{m=0}^{L_d-1} \frac{e^{-\delta}\delta^{L_d-1-m}}{\Gamma(L_d - m)}V\left(\frac{1}{\delta}\right). \tag{21}
$$

Proof 5: When $P \to \infty$, we have $a \to \infty$ and $c \to \infty$. Following (19), $\lim_{P \to \infty} R_s^*(\mu) = \log\frac{c\mu^2 r_d^{-\alpha}}{a\varpi} = \log\frac{\mu^2 L_e r_d^{-\alpha}}{L_d\varpi}$. By exploiting the same integration method as Theorem 2, we derive the result given in (21). Since $\delta = \sqrt{\frac{\varpi L_d r_d^\alpha}{L_e}}$ is independent of P, we have that τ^* is independent of P when $P \to \infty$.

V. SECRECY PERFORMANCE OF AN BEAMFORMING

In this section, we first investigate the connection and secrecy outage performance of AN beamforming. Then we maximize the secrecy throughput under a given SOP constraint and derive the optimal power allocation ratio η^*.

A. Connection Probability

Given $\xi_d^{AN} = \eta c\mu r_d^{-\alpha}$, from (10), the connection probability of AN beamforming can be given by

$$\mathcal{P}_c = \frac{1}{\Gamma(L_d)}\Gamma\left(L_d, \frac{(2^{R_t}-1)r_d^\alpha}{\eta c}\right). \tag{22}$$

B. Secrecy Outage Performance

1) Non-Colluding Eavesdroppers: Define $v \triangleq \|\mathbf{g}_{kn}\|^2$, we have $v \sim \text{Gamma}(L_e - L_c, 1)$. Since $\Omega_c \cap \Omega_n = \emptyset$, u and v are independent to each other. The CDF of ξ_k^{AN} can be given by

$$F_{\xi_k}(x) = 1 - \mathbb{E}_v\left[e^{-\frac{(1-\eta)\mu x}{\eta\mu_c(N_t-L_d)}v - \frac{\mu x r_k^\alpha}{\eta a\mu_c}}\right]$$

$$\overset{(e)}{=} 1 - e^{-\frac{\mu x r_k^\alpha}{\eta a\mu_c}}\left[1 + \frac{(1-\eta)\mu x}{\eta\mu_c(N_t-L_d)}\right]^{-(L_e-L_c)}, \tag{23}$$

where (e) holds for the integration formula [40, 3.326.2]. The CDF of ξ_e can be calculated as

$$F_{\xi_e}(x) = \mathbb{E}_{\Phi_e, \{\mu_c\}}\left[\prod_{e_k \in \Phi_e}\mathbb{P}\{\xi_k < x\}\right]$$

$$= \exp\left\{-\lambda\int_0^\infty\int_0^{2\pi}\mathbb{E}_{\mu_c}\left\{\left[1 + \frac{(1-\eta)\mu x}{\eta\mu_c(N_t-L_d)}\right]^{-(L_e-L_c)}\right.\right.$$

$$\left.\left.\times e^{-\frac{\mu x r_k^\alpha}{\eta a\mu_c}}\right\} r_k d\theta dr_k\right\}$$

$$= \exp\left\{-\pi\lambda\Gamma\left(\frac{2}{\alpha}+1\right)\left(\frac{\mu x}{\eta a}\right)^{-\frac{2}{\alpha}}\sum_{L_c=1}^{L_l}p(L_c)\right.$$

$$\left.\times\mathbb{E}_{\mu_c}\left\{\left[1 + \frac{(1-\eta)\mu x}{\eta\mu_c(N_t-L_d)}\right]^{-(L_e-L_c)}\left(\frac{1}{\mu_c}\right)^{-\frac{2}{\alpha}}\right\}\right\}. \tag{24}$$

Denoting $b \triangleq \frac{(1-\eta)\mu x}{\eta(N_t-L_d)}$ yields

$$F_{\xi_e}(x) = \exp\left\{-\pi\lambda\Gamma\left(\frac{2}{\alpha}+1\right)\left(\frac{\mu x}{\eta a}\right)^{-\frac{2}{\alpha}}\sum_{L_c=1}^{L_l}p(L_c)\right.$$

$$\left.\times\int_0^\infty(\mu_c+b)^{-(L_e-L_c)}\mu_c^{L_e-L_c+\frac{2}{\alpha}}\frac{\mu_c^{L_c-1}}{\Gamma(L_c)}e^{-\mu_c}d\mu_c\right\}$$

$$\overset{(f)}{=} \exp\left\{-\pi\lambda\Gamma\left(\frac{2}{\alpha}+1\right)\left(\frac{\mu x}{\eta a}\right)^{-\frac{2}{\alpha}}\sum_{L_c=1}^{L_l}\frac{p(L_c)e^b}{\Gamma(L_c)}\right.$$

$$\left.\times\int_b^\infty y^{-(L_e-L_c)}(y-b)^{L_e+\frac{2}{\alpha}-1}e^{-y}dy\right\}$$
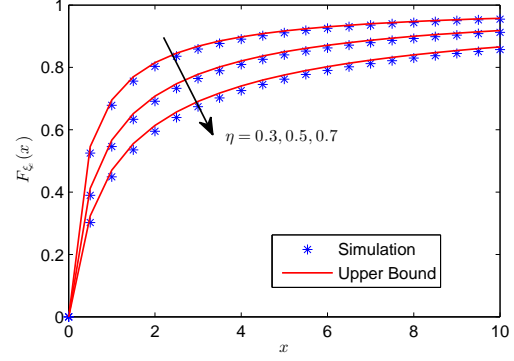
Fig. 4. $F_{\xi_e}(x)$ versus x for different η's, with $N_t = 100$, $L_d = 20$, $L_e = 20$, $\alpha = 4$, $\lambda = 1$ and $P = 0$dBm.

$$\overset{(g)}{=} \exp\left\{-\pi\lambda\Gamma\left(\frac{2}{\alpha}+1\right)\Gamma\left(\frac{2}{\alpha}+L_e\right)\left(\frac{\mu x}{\eta a}\right)^{-\frac{2}{\alpha}}\right.$$

$$\left.\times\sum_{L_c=1}^{L_l}\frac{p(L_c)e^{\frac{b}{2}}b^{\frac{L_c+\frac{2}{\alpha}-1}{2}}}{\Gamma(L_c)}W_{\frac{L_c-2L_e-\frac{2}{\alpha}+1}{2}, \frac{-L_c-\frac{2}{\alpha}}{2}}(b)\right\}, \tag{25}$$

where (f) follows from the variable transformation $y = \mu_c + b$ and (g) holds for the integration formula [40, 3.383.4]. Since the formula inside the mathematical expectation in (24) is a convex function of $\frac{1}{\mu_c}$, using Jensen's inequality yields

$$F_{\xi_e}(x) \leq \exp\left\{-\pi\lambda\Gamma\left(\frac{2}{\alpha}+1\right)\left(\frac{\mu x}{\eta a}\right)^{-\frac{2}{\alpha}}\sum_{L_c=1}^{L_l}p(L_c)\right.$$

$$\left.\times\left[1 + \frac{(1-\eta)\mu x}{\eta(N_t-L_d)}\mathbb{E}_{\mu_c}\left(\frac{1}{\mu_c}\right)\right]^{-(L_e-L_c)}\left[\mathbb{E}_{\mu_c}\left(\frac{1}{\mu_c}\right)\right]^{-\frac{2}{\alpha}}\right\}$$

$$= \exp\left\{-\pi\lambda\Gamma\left(\frac{2}{\alpha}+1\right)\left(\frac{\mu x}{\eta a}\right)^{-\frac{2}{\alpha}}\sum_{L_c=1}^{L_l}p(L_c)(L_c-1)^{\frac{2}{\alpha}}\right.$$

$$\left.\times\left[1 + \frac{(1-\eta)\mu x}{\eta(N_t-L_d)(L_c-1)}\right]^{-(L_e-L_c)}\right\}. \tag{26}$$

The above formula (26) gives an upper bound of $F_{\xi_e}(x)$. In order to verify the accuracy of (26), we plot $F_{\xi_e}(x)$ in (26) versus x for different values of η in Fig. 4. We find that the upper-bound curves coincide well with simulation ones, and they are very tight. Thus we use the result in (26) instead of (25) in the following deductions.

Then the SOP of AN beamforming can be expressed as

$$\mathcal{P}_{so}(\mu) = 1 - \exp\left\{-\pi\lambda\Gamma\left(\frac{2}{\alpha}+1\right)\right.$$

$$\times\left\{\frac{\mu[\eta c\mu r_d^{-\alpha}-(T-1)]}{\eta aT}\right\}^{-\frac{2}{\alpha}}\sum_{L_c=1}^{L_l}p(L_c)(L_c-1)^{\frac{2}{\alpha}}$$

$$\left.\times\left[1 + \frac{\mu(1-\eta)[\eta c\mu r_d^{-\alpha}-(T-1)]}{\eta T(N_t-L_d)(L_c-1)}\right]^{-(L_e-L_c)}\right\}. \tag{27}$$

2) Colluding Eavesdroppers: In this scenario,

$$\mathcal{P}_{so}(\mu) = \mathbb{P}\{\sum_{e_k \in \Phi_e} \frac{\frac{\eta a \mu_c r_k^{-\alpha}}{\mu} u}{\frac{(1-\eta)a r_k^{-\alpha}}{N_t - L_d} v + 1} > \frac{\eta c \mu r_d^{-\alpha} - (T-1)}{T}\} = $$

$$\mathbb{P}\left\{ I_e > \frac{\eta c \mu r_d^{-\alpha} - (T-1)}{T} \right\}, \text{ where } I_e \triangleq \sum_{e_k \in \Phi_e} \frac{z_2 \mu_c u}{z_3 v + r_k^{\alpha}} \text{ with}$$

$z_2 \triangleq \frac{\eta a}{\mu}$ and $z_3 \triangleq \frac{(1-\eta)a}{N_t - L_d}$. Then we derive a closed-form expression for $\mathcal{L}_{I_e}(s)$ in the following lemma.

Lemma 2: The Laplace transform of I_e can be given by

$$\mathcal{L}_{I_e}(s) = \exp\left\{ -\pi\lambda\Gamma(1+2\alpha)\Gamma(1-2\alpha)\frac{\Gamma(L_e - 2\alpha)}{\Gamma(L_e + \frac{3}{2})} z_3^{-2\alpha-1} \right.$$

$$\left. \times z_2 s \sum_{L_c=1}^{L_l} p(L_c) L_c F\left(L_c + 1, 2\alpha + 1; L_e + \frac{3}{2}; -\frac{s z_2}{z_3} \right) \right\}. \tag{28}$$

Proof 6: Please see Appendix B.

Following Theorem 1, in the scenario of colluding eavesdroppers, the SOP of AN beamforming can be approximated as

$$\mathcal{P}_{so} \gtrapprox \sum_{n=0}^{N} \binom{N}{n} (-1)^n \mathcal{L}_{I_e}\left(\frac{qTn}{\eta c \mu r_d^{-\alpha} - (T-1)} \right). \tag{29}$$

C. Secrecy Throughput Maximization and Optimal Power Allocation

In this subsection, we optimize η to get a maximum secrecy throughput under the SOP constraint for the AN scheme in the non-colluding eavesdroppers scenario.

According to (18) and by denoting $\rho(\eta) \triangleq \frac{F_{\xi_e}^{-1}(1-\epsilon)}{\eta}$ for the AN scheme, the optimization problem can be formulated as

$$\max_{\eta} \quad R_s(\mu) = \log\frac{1 + \eta c \mu r_d^{-\alpha}}{1 + \eta \rho(\eta)}, \tag{30}$$

$$s.t. \quad 0 \le \eta \le 1, \ \rho(\eta) < c \mu r_d^{-\alpha},$$

where $\rho(\eta) < c \mu r_d^{-\alpha}$ is the transmission constraint of the on-off transmission scheme that guarantees a positive $R_s(\mu)$.

Rewriting the definition formula of $\rho(\eta)$ as $F_{\xi_e}^{AN}(\eta\rho(\eta)) = 1 - \epsilon$, we derive $J(\rho) - Q = 0$, where $J(\rho) \triangleq \rho^{-\frac{2}{\alpha}} \sum_{L_c=1}^{L_l} z_4[1 + z_5(1-\eta)\rho]^{-(L_e - L_c)}$ and $Q \triangleq -\frac{\ln(1-\epsilon)(\frac{\mu}{a})^{\frac{2}{\alpha}}}{\pi\lambda\Gamma(\frac{2}{\alpha}+1)}$, with $z_4 \triangleq p(L_c)(L_c - 1)^{\frac{2}{\alpha}}$, $z_5 \triangleq \frac{\mu}{(N_t - L_d)(L_c - 1)}$. It is hard to get a analytical expression of $\rho(\eta)$ for the AN scheme. Instead, we investigate the relationship between $\rho(\eta)$ and η in the following lemma in order to find an efficient way to calculate ρ with a given η.

Lemma 3: $\rho(\eta)$ is a monotonically increasing and convex function of η in the range $\eta \in [0, 1]$.

Proof 7: Please see Appendix C.

From the definition of ρ, we easily obtain that $\rho \ge 0$. Due to Lamma 3, the maximum ρ is achieved at $\eta = 1$. Then we can obtain $\rho_{\max} = Q^{-\frac{\alpha}{2}}(\sum_{L_c=1}^{L_l} z_4)^{\frac{\alpha}{2}}$ from $J(\rho) - Q = 0$. We define $\Xi(\rho) \triangleq J(\rho)^{-1} - Q^{-1} = 0$. Evidently, for an given η, $\Xi(\rho)$ is a monotonically increasing function of ρ. Since $\Xi(0) = -Q^{-1} < 0$ and $\Xi(\rho_{\max}) = Q^{-1}\{\sum_{L_c=1}^{L_l} z_4\{\sum_{L_c=1}^{L_l} z_4[1 + z_5(1-\eta)Q^{-\frac{\alpha}{2}}(\sum_{L_c=1}^{L_l} z_4)^{\frac{\alpha}{2}}]^{-(L_e - L_c)}\}^{-1} - 1\} \ge 0$, we find that $\Xi(\rho)$ has the unique zero-crossing point. Therefore, we

can obtain the unique root ρ of $\Xi(\rho) = 0$ by utilizing the bisection method within the range $[0, \rho_{\max}]$.

Theorem 3: Given $\rho < c \mu r_d^{-\alpha}$, R_s is a concave function of η. The optimal η^* that maximizes R_s is given by

$$\eta^* = \begin{cases} 1, & \frac{c \mu r_d^{-\alpha}}{1 + c \mu r_d^{-\alpha}} - \frac{\rho_{\max} + \frac{\alpha\mu}{2(N_t - L_d)}\rho_{\max}^2}{1 + \rho_{\max}} > 0, \\ \eta^\star, & \text{otherwise}, \end{cases} \tag{31}$$

where $\eta^\star$ is the unique root of the following equation

$$\frac{dR_s}{d\eta} = \frac{1}{\ln 2}\left(\frac{c \mu r_d^{-\alpha}}{1 + \eta c \mu r_d^{-\alpha}} - \frac{\rho + \eta\frac{d\rho}{d\eta}}{1 + \eta\rho} \right) = 0, \tag{32}$$

with $\frac{d\rho}{d\eta}$ defined in (36).

Proof 8: Please see Appendix D.

The above theorem provides the solution of the optimization problem (30), and supplies an efficient approach, i.e., the bisection method, that can be used to search the optimal $\eta^\star$, due to the concavity of R_s on η. Then we investigate how the optimal power allocation ratio $\eta^\star$ varies in different scenarios in the following corollary.

Corollary 3: The optimal $\eta^\star$ monotonically decreases with λ and r_d, and monotonically increases with ϵ.

Proof 9: Please see Appendix E.

Corollary 3 indicates that when the transmission is more vulnerable to eavesdropping, i.e., with a poorer quality of the destination's channel, in a denser eavesdroppers scenario or under a more rigorous SOP constraint, we should allocate more power to AN.

Next, we calculate the transmission threshold δ. We have already derived the transmission constraint $\rho(\eta) < c \mu r_d^{-\alpha}$ to guarantee a positive R_s. Since $\rho(\eta)$ monotonically increases with η, if $\rho(0)$, the minimum $\rho(\eta)$, is not below $c \mu r_d^{-\alpha}$, i.e., $\rho(0) \ge c \mu r_d^{-\alpha} \Rightarrow \mu \le \frac{r_d^\alpha \rho(0)}{c}$, the transmission constraint $\rho(\eta) < c \mu r_d^{-\alpha}$ can not be satisfied. Hence we can not find a feasible η to maintain the positivity of R_s. Therefore, $\mu > \frac{r_d^\alpha \rho(0)}{c}$ must be guaranteed, and as a consequence we set $\delta = \frac{r_d^\alpha \rho(0)}{c}$, which corresponds to an on-off transmission, i.e., when $\mu > \delta$, the transmitter radiates signals with $R_s^*(\mu)$; otherwise, the transmission suspends and we set $R_s(\mu) = 0$.

From (5), the maximum secrecy throughput of AN beamforming can be given by

$$\tau^* = \int_{\frac{r_d^\alpha \rho(0)}{c}}^{\infty} R_s^*(\mu) f_\mu(x) dx, \tag{33}$$

where $f_\mu(x) = \frac{x^{(L_d - 1)}}{\Gamma(L_d)} e^{-x}$.

VI. NUMERICAL RESULTS

In this section, numerical results are presented to verify our theoretical analysis. The transmitter is equipped with an ULA containing 100 antennas. We set the pass loss exponent $\alpha = 4$ and the noise power $\sigma_n^2 = -60$dBm [30], [33], [35].
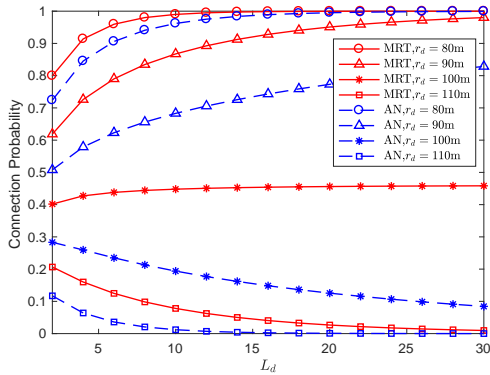
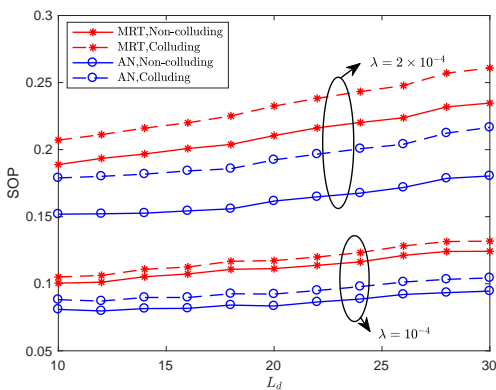Fig. 5. Connection probability versus L_d for different r_d's, with $P = 10$dBm, $R_t = 6$ and $\eta = 0.8$.

Fig. 6. SOP versus L_d for different λ's, with $N_t = 100$, $P = 0$dBm, $r_d = 50$m, $L_e = 20$, $\eta = 0.5$ and $R_s = 4$.

Fig. 7. Optimal power allocation ratio η^* versus L_d for different r_d's, with $N_t = 100$, $P = 10$dBm, $L_e = 20$, $\lambda = 5 \times 10^{-6}$ and $\epsilon = 0.01$.

Fig. 8. Optimal power allocation ratio η^* versus λ for different L_e's, with $N_t = 100$, $P = 10$dBm, $L_d = 20$, $r_d = 50$m and $\epsilon = 0.01$.

A. Connection and Secrecy Outage Performance

Fig. 5 describes connection probability versus L_d for different values of r_d. We find that when r_d is small, connection probability increases as the number of resolvable paths L_d increases. The trend is opposite when r_d is large. The underlying reason is that when the number of paths becomes larger, the influence of paths with either very high or very low gain becomes weaker, i.e., the received power is closer to its mean and the randomness is smaller. When r_d is small, the mean of SNR is high. Therefore, with the increase of L_d, SNR is closer to its higher mean and the connection probability will increase. Otherwise, when r_d is large, SNR approaches to its lower mean and the connection probability will decrease. We also observe that connection probability of AN beamforming is lower than that of MRT beamforming due to the fact that partial transmit power is allocated to the AN transmission.

Fig. 6 presents $\mathcal{P}_{so}$ versus L_d for different values of λ. As shown in the figure, $\mathcal{P}_{so}$ is higher in colluding eavesdroppers scenario than that in non-colluding eavesdroppers scenario. The differences are more obvious when eavesdroppers are denser. For both AN beamforming and MRT beamforming, $\mathcal{P}_{so}$ decreases when L_d reduces. The underlying reason is that when the number of the destination's resolvable paths L_d drops, the information signal is transmitted through fewer
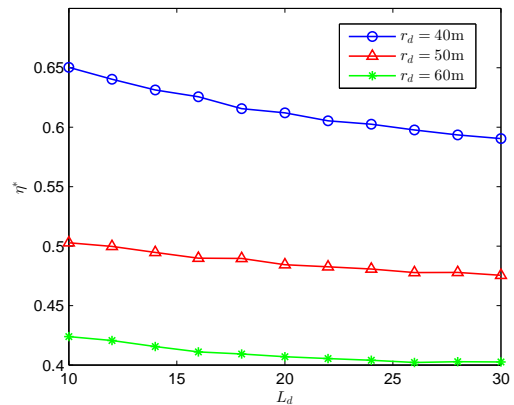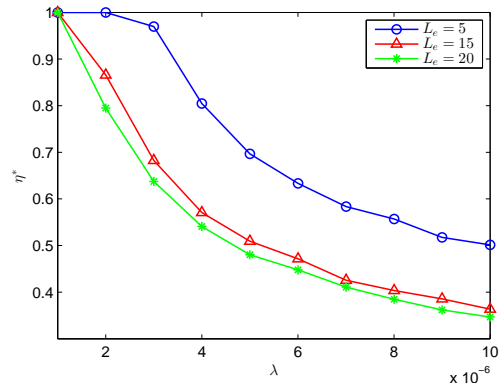
directions, which leads to a lower chance of confidential message leakage.

B. Optimal Power Allocation of AN Beamforming

Fig. 7 investigates the optimal power allocation ratio η^* that maximizes the secrecy throughput versus L_d for different values of r_d. we find that η^* increases with the decrease of r_d. The figure also shows that for a given $L_e = 20$, when L_d varies from 10 to 30, η^* is getting smaller. It is because that when L_d becomes larger, the transmit beam of the information signals covers more spatially resolvable directions, so that eavesdroppers' resolvable paths are more likely to fall into that beam, which means that eavesdroppers will receive more information signals. Thus we should give a larger fraction of transmit power to AN transmission in order to interfere with eavesdroppers.

Fig. 8 plots the optimal power allocation ratio η^* that maximizes the secrecy throughput versus λ for different values of L_e. As shown in the figure, η^* decreases as λ increases, which implies that we should increase AN power when secure transmissions become more vulnerable to intercepting. In addition, the value of η^* falls down with an increase in L_e. The underlying reason is that when L_e becomes larger, resolvable
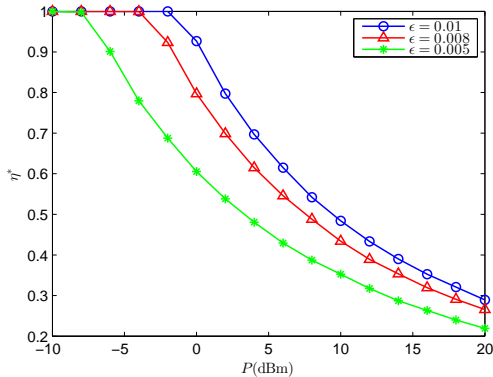
Fig. 9. Optimal power allocation ratio η^* versus P for different ϵ's, with $N_t = 100$, $P = 10$dBm, $L_d = 20$, $L_e = 20$, $r_d = 50$m and $\lambda = 5 \times 10^{-6}$.

Fig. 11. Secrecy throughput versus L_e for different λ's, with $N_t = 100$, $P = 10$dBm, $L_d = 20$, $r_d = 50$m and $\epsilon = 0.01$.
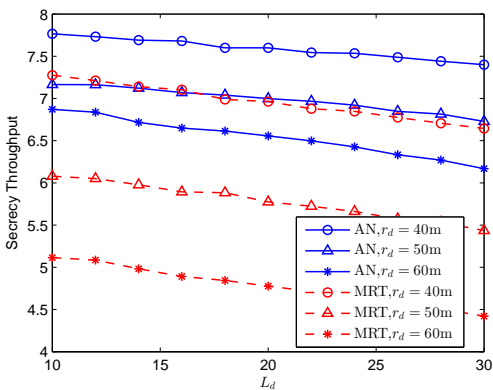

Fig. 10. Secrecy throughput versus L_d for different r_d's, with $N_t = 100$, $P = 10$dBm, $L_e = 20$, $\lambda = 5 \times 10^{-6}$ and $\epsilon = 0.01$.

paths of eavesdroppers and those of the destination are more likely to overlap, and then eavesdroppers are able to wiretap more confidential messages. Therefore, more power is ought to be allocated to AN transmission in order to deteriorate eavesdroppers' channels.

Fig. 9 illustrates the optimal power allocation ratio η^* that maximizes the secrecy throughput versus P for different values of ϵ. η^* keeps 1 at the low transmit power region and then drops as P increases, which implies that we should transmit information signals with full power to achieve a higher message rate at the low power regime and give a larger fraction of power to AN transmission when the transmit power becomes higher. We also find that for a given transmit power P, as ϵ decreases, η^* decreases.

C. Secrecy Throughput Performance

Fig. 10 describes the secrecy throughput versus L_d for different values of r_d. Secrecy throughput becomes higher with the decrease of r_d, which confirms the fact that a better destination's channel contributes to a promotion of secrecy throughput. We also find that the secrecy throughput increases as L_d decreases. The underlying reason is that confidential signals are radiated through all the directions of the destination's resolvable paths. In the small L_d scenario, the transmit
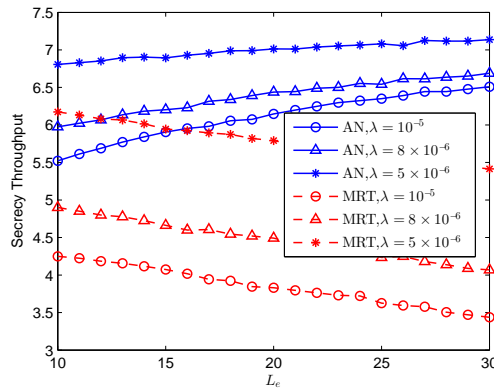
beam which contains secrecy messages is narrow. It is hard for eavesdroppers to intercept. Therefore, smaller L_d is beneficial for enhancing the secrecy throughput.

Fig. 11 presents the secrecy throughput versus L_e for different values of λ. We observe that the secrecy throughput increases with a smaller λ for both transmission schemes, which indicates that secrecy performance improves in a sparse eavesdropper scenario. As the number of the eavesdropper's resolvable paths L_e changes, the variation tendencies of MRT beamforming and AN beamforming are different. For MRT beamforming, the secrecy throughput turns to be lower as L_e increases. It is because that in the large L_e situation, eavesdroppers' resolvable paths are more likely to cover the destination's resolvable paths in which directions the information signals emit. Thus eavesdroppers overhear more secrecy messages and the secrecy performance will be poorer. Although a heavier leakage to eavesdroppers also happens in the AN beamforming case when L_e grows, the transmitter gives more power to AN transmission as shown in Fig. 8, so that the interference received by eavesdroppers increases too. With the transmission of AN, the SINR of eavesdroppers may drop. Therefore, the results in the figure show that the secrecy throughput increases when L_e increases for the AN scheme. In addition, we observe that the gap between the secrecy throughput of AN beamforming and that of MRT beamforming is more evident in the denser eavesdropper scenario.

Fig. 12 describes the secrecy throughput versus P for different values of ϵ. Obviously, by increasing transmit power P, the secrecy throughput increases. We also see that MRT beamforming presents a comparable performance to AN beamforming in the low transmit power scenario. As revealed in Corollary 2, the secrecy throughput of MRT beamforming at the high transmit power regime converges to a constant which is irrespective to P. However, since more power is allocated to the AN transmission to confuse eavesdroppers as shown in Fig. 9, the secrecy throughput of AN beamforming keeps increasing, and the superiority of AN beamforming becomes more obvious. Meanwhile, as the increase of the SOP constraint threshold ϵ, the secrecy throughput becomes higher.
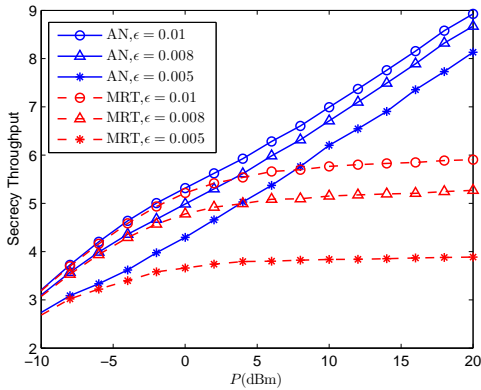
Fig. 12. Secrecy throughput versus P for different ϵ's, with $N_t = 100$, $P = 10$dBm, $L_d = 20$, $L_e = 20$, $r_d = 50$m and $\lambda = 5 \times 10^{-6}$.

VII. CONCLUSION

This paper has comprehensively studied secure transmissions in millimeter wave systems where the locations of eavesdroppers are modeled as an independent homogeneous PPP. We have established a discrete angular domain channel model which characterized by spatially resolvable paths to facilitate the theoretical design and analysis of secure transmission schemes. Then we have evaluated the performance of MRT beamforming and AN beamforming by obtaining the connection probability, the SOP and the secrecy throughput. Particularly, we have derived the optimal power allocation between AN and the information signal that maximizes the secrecy throughput for AN beamforming. Through our analysis, we have revealed that the superiority of AN beamforming over MRT beamforming is highly significant in dense eavesdroppers scenario, at the high transmit power regime or in the situation that the number of the eavesdropper's spatially resolvable paths is large.

APPENDIX A
PROOF OF THEOREM 2

Since $\mu \sim \text{Gamma}(L_d, 1)$, the PDF of μ can be given by $f_\mu(x) = \frac{x^{(L_d-1)}}{\Gamma(L_d)}e^{-x}$. By substituting (19), we derive the maximum secrecy throughput of MRT beamforming as

$$\tau^* = \int_\delta^\infty R_s^*(x)f_\mu(x)dx$$
$$\overset{(h)}{=} \int_0^\infty \frac{1}{\Gamma(L_d)} \log \frac{(y+\delta)[1+cr_d^{-\alpha}(y+\delta)]}{y+\delta+z_1}$$
$$\times (y+\delta)^{L_d-1}e^{-(y+\delta)}dy$$
$$= \frac{e^{-\delta}}{\Gamma(L_d)} \sum_{m=0}^{L_d-1} \binom{L_d-1}{m}\delta^{L_d-1-m} \int_0^\infty \left[\log(1+\frac{1}{\delta}y)\right.$$
$$+ \log(1+\frac{cr_d^{-\alpha}}{1+cr_d^{-\alpha}\delta}y) - \log(1+\frac{1}{\delta+z_1}y)$$
$$\left. + \log\frac{\delta(1+cr_d^{-\alpha}\delta)}{\delta+z_1}\right] y^m e^{-y}dy,$$

(34)

where (h) holds for the transformation $y = x - \delta$. According to [40, 4.337.5], the final result shown in (20) is obtained.

APPENDIX B
PROOF OF LEMMA 2

$$\mathcal{L}_{I_e}(s) = \mathbb{E}_{\Phi_e,u,v,\mu_c}\left[e^{-s\sum_{e_k\in\Phi_e}\frac{z_2\mu_c u}{z_3v+r_k^\alpha}}\right]$$
$$= \exp\left\{-2\pi\lambda\sum_{L_c=1}^{L_l} p(L_c)\mathbb{E}_{u,v,\mu_c}\left[\int_0^\infty [1\right.\right.$$
$$\left.\left.- \exp\left(-s\frac{z_2\mu_c u}{z_3v+r_k^\alpha}\right)\right]r_k dr_k\right]\right\}$$
$$= \exp\left\{-2\pi\lambda\sum_{L_c=1}^{L_l} p(L_c)\int_0^\infty\int_0^\infty\int_0^\infty sz_2\mu_c\right.$$
$$\left.\times(r_k^\alpha + sz_2\mu_c + z_3v)^{-1}r_k dr_k f(v)f(\mu_c)dvd\mu_c\right\}$$
$$\overset{(i)}{=} \exp\left\{-\pi\lambda\Gamma(1+2\alpha)\Gamma(1-2\alpha)\sum_{L_c=1}^{L_l} p(L_c)\right.$$
$$\left.\times\int_0^\infty\int_0^\infty sz_2\mu_c(sz_2\mu_c+z_3v)^{-2\alpha-1}f(v)f(\mu_c)dvd\mu_c\right\}$$
$$\overset{(j)}{=} \exp\left\{-\pi\lambda\Gamma(1+2\alpha)\Gamma(1-2\alpha)z_3^{-\frac{L_e-L_c}{2}-\alpha}(sz_2)^{\frac{L_e-L_c}{2}-\alpha}\right.$$
$$\times\sum_{L_c=1}^{L_l} p(L_c)\int_0^\infty \mu_c^{\frac{L_e-L_c}{2}-\alpha}e^{\frac{sz_2\mu_c}{2z_3}}$$
$$\left.\times W_{\frac{-L_e+L_c}{2}-\alpha,\frac{1-L_e+L_c}{2}+\alpha}\left(\frac{sz_2\mu_c}{z_3}\right)f(\mu_c)d\mu_c\right\},$$

(35)

where $f(u) = e^{-u}$, $f(v) = \frac{v^{(L_e-L_c-1)}}{\Gamma(L_e-L_c)}e^{-v}$ and $f(\mu_c) = \frac{\mu_c^{(L_c-1)}}{\Gamma(L_c)}e^{-\mu_c}$ are PDFs of u, v and μ_c respectively, (i) holds for the transformation $x = r_k^\alpha$ and the integration formula [40, 3.194], (j) holds for the transformation $y = z_3v + sz_2\mu_c$ and the integration formula [40, 3.383.4]. By utilizing the integration formula [40, 7.621.3], we obtain the result in (28).

APPENDIX C
PROOF OF LEMMA 3

The first-order and second-order derivatives of $\rho(\eta)$ can be given by

$$\frac{d\rho}{d\eta} = -\frac{\partial J/\partial\eta}{\partial J/\partial\rho} = \frac{\rho^2}{\rho(1-\eta)+\frac{2}{\alpha}\sigma},$$

(36)

$$\frac{d^2\rho}{d\eta^2} = \frac{2}{\rho}\left(\frac{d\rho}{d\eta}\right)^2 + \frac{\rho^2[\varsigma - \frac{2}{\alpha}\frac{d\sigma}{d\eta}]}{[\rho(1-\eta)+\frac{2}{\alpha}\sigma]^2},$$

(37)

where $\sigma \triangleq \frac{\sum_{L_c=1}^{L_l} z_4[1+z_5(1-\eta)\rho]^{-(L_e-L_c)}}{\sum_{L_c=1}^{L_l} z_4z_5(L_e-L_c)[1+z_5(1-\eta)\rho]^{-(L_e-L_c)-1}}$, and $\varsigma \triangleq \rho - (1-\eta)\frac{d\rho}{d\eta}$. Since $\sigma > 0$, obviously, $\frac{d\rho}{d\eta} > 0$. By substituting (36), we have $\varsigma = \frac{\frac{2}{\alpha}\sigma\rho}{\rho(1-\eta)+\frac{2}{\alpha}\sigma} > 0$. Denoting

$C_1 \triangleq \sum_{L_c=1}^{L_l} z_4 z_5 (L_e - L_c)[1 + z_5(1-\eta)\rho]^{-(L_e-L_c)-1}$ and $C_2 \triangleq \sum_{L_c=1}^{L_l} z_4[1 + z_5(1-\eta)\rho]^{-(L_e-L_c)}$, we have

$$
\begin{aligned}
\frac{d\sigma}{d\eta} &= \frac{\frac{dC_2}{d\eta}}{C_1} - \frac{C_2 \frac{dC_1}{d\eta}}{C_1^2} \\
&= \frac{1}{C_1^2}\Big\{ C_1 \sum_{L_c=1}^{L_l} z_4 z_5 (L_e - L_c)[1 + z_5(1-\eta)\rho]^{-(L_e-L_c)-1}\varsigma \\
&\quad - C_2 \sum_{L_c=1}^{L_l} z_4 z_5^2 (L_e - L_c)(L_e - L_c + 1) \\
&\quad \times [1 + z_5(1-\eta)\rho]^{-(L_e-L_c)-2}\varsigma \Big\} \\
&< \frac{\varsigma}{C_1^2}\{ C_1^2 - C_2 C_3 \} \overset{(k)}{\le} 0,
\end{aligned}
\tag{38}
$$

where $C_3 \triangleq \sum_{L_c=1}^{L_l} z_4 z_5^2 (L_e - L_c)^2 [1 + z_5(1-\eta)\rho]^{-(L_e-L_c)-2}$ and (k) holds for the Holder's inequality $(\sum xy)^2 \le (\sum x^2)(\sum y^2)$ with $x = \{z_4[1 + z_5(1-\eta)\rho]^{-(L_e-L_c)}\}^{\frac{1}{2}}$ and $y = \{z_4 z_5^2 (L_e - L_c)^2 [1 + z_5(1-\eta)\rho]^{-(L_e-L_c)-2}\}^{\frac{1}{2}}$. Thus we have that $\frac{d^2\rho}{d\eta^2} > \frac{2}{\rho}\left(\frac{d\rho}{d\eta}\right)^2 > 0$. With $\frac{d\rho}{d\eta} > 0$ and $\frac{d^2\rho}{d\eta^2} > 0$, we complete the proof.

APPENDIX D
PROOF OF THEOREM 3

The second-order derivative of R_s can be described as

$$
\begin{aligned}
\frac{d^2 R_s}{d\eta^2} = -\frac{1}{\ln 2}\Big\{ & \frac{(c\mu r_d^{-\alpha})^2}{(1 + \eta c\mu r_d^{-\alpha})^2} + \frac{1}{(1+\eta\rho)^2} \\
& \times \left[(1+\eta\rho)\left(2\frac{d\rho}{d\eta} + \eta\frac{d^2\rho}{d\eta^2}\right) - \left(\rho + \eta\frac{d\rho}{d\eta}\right)^2 \right] \Big\},
\end{aligned}
\tag{39}
$$

with $\frac{d\rho}{d\eta}$ and $\frac{d^2\rho}{d\eta^2}$ given by (36) and (37). Substituting $\frac{d^2\rho}{d\eta^2} > \frac{2}{\rho}\left(\frac{d\rho}{d\eta}\right)^2 > 0$ (see Appendix C) into the above equation yields $\frac{d^2 R_s}{d\eta^2} < -\frac{1}{\ln 2}\left[\frac{(c\mu r_d^{-\alpha})^2}{(1+\eta c\mu r_d^{-\alpha})^2} - \frac{\rho^2}{(1+\eta\rho)^2}\right]$. Since $c\mu r_d^{-\alpha} > \rho$, we have $\frac{d^2 R_s}{d\eta^2} < 0$, i.e., R_s is a concave function of η.

For the concavity of R_s, the maximum value of R_s is achieved either at the boundaries or at the zero-crossing point of $\frac{dR_s}{d\eta}$. From the first-order derivative formula of R_s in (32), we obtain $\frac{dR_s}{d\eta}|_{\eta=0} = \frac{1}{\ln 2}(c\mu r_d^{-\alpha} - \rho) > 0$ and $\frac{dR_s}{d\eta}|_{\eta=1} = \frac{1}{\ln 2}\left\{ \frac{c\mu r_d^{-\alpha}}{1 + c\mu r_d^{-\alpha}} - \frac{\rho_{\max} + \frac{\alpha\mu}{2(N_t - L_d)}\rho_{\max}^2}{1 + \rho_{\max}} \right\}$. If $\frac{dR_s}{d\eta}|_{\eta=1} > 0$, R_s monotonically increases with η, and the optimal value of η is 1 with the condition directly obtained from $\frac{dR_s}{d\eta}|_{\eta=1} > 0$. If $\frac{dR_s}{d\eta}|_{\eta=1} \le 0$, R_s first increases and then decreases, and the optimal value of η is the unique root of $\frac{dR_s}{d\eta}$.

APPENDIX E
PROOF OF COROLLARY 3

Substituting (36) into (32) and denoting $\hat{c} \triangleq c\mu r_d^{-\alpha}$ yield

$$
(\hat{c}\eta^2 + 1)\rho^2 + (\hat{c}\eta + \frac{2}{\alpha}\sigma - \hat{c})\rho - \frac{2}{\alpha}\sigma\hat{c} = 0. \tag{40}
$$

Denote the left side of the above equation as Y, we obtain

$$
\frac{\partial Y}{\partial \eta} = z_6 \frac{d\rho}{d\eta} + \frac{2}{\alpha}(\rho - \hat{c})\frac{d\sigma}{d\eta} + 2\hat{c}\eta\rho^2 + \hat{c}\rho > 0, \tag{41}
$$

where $z_6 \triangleq 2\hat{c}\eta^2\rho + 2\rho + \hat{c}\eta + \frac{2}{\alpha}\sigma - \hat{c}$. By substituting (40), we have $z_6 = \rho + \hat{c}\eta^2\rho + \frac{2}{\alpha}\hat{c}\sigma\frac{1}{\rho} > 0$. From $\rho < \hat{c}$ and $\frac{d\sigma}{d\eta} < 0$, we derive $\frac{\partial Y}{\partial \eta} > 0$.

1) λ: $\frac{d\eta}{d\lambda} = -\frac{\partial Y/\partial\lambda}{\partial Y/\partial\eta} = -\frac{z_6\frac{d\rho}{d\lambda}}{\partial Y/\partial\eta}$, where $z_6 > 0$ and $\frac{\partial Y}{\partial\eta} > 0$. From the definition of Ξ, we find $\Xi = 0$, $\frac{\partial\Xi}{\partial\rho} > 0$ and $\frac{\partial\Xi}{\partial\lambda} < 0$, hence $\frac{d\rho}{d\lambda} = -\frac{\partial\Xi/\partial\lambda}{\partial\Xi/\partial\rho} > 0$. Thus we derive $\frac{d\eta}{d\lambda} < 0$.

2) ϵ: $\frac{d\eta}{d\epsilon} = -\frac{\partial Y/\partial\epsilon}{\partial Y/\partial\eta} = -\frac{z_6\frac{d\rho}{d\epsilon}}{\partial Y/\partial\eta}$, where $z_6 > 0$ and $\frac{\partial Y}{\partial\eta} > 0$. Since $\frac{\partial\Xi}{\partial\epsilon} > 0$, we have $\frac{d\rho}{d\epsilon} = -\frac{\partial\Xi/\partial\epsilon}{\partial\Xi/\partial\rho} < 0$. Thus we obtain $\frac{d\eta}{d\epsilon} > 0$.

3) r_d: $\frac{d\eta}{dr_d} = -\frac{\partial Y/\partial r_d}{\partial Y/\partial\eta} = -\frac{\frac{\partial Y}{\partial\hat{c}}\frac{d\hat{c}}{dr_d}}{\partial Y/\partial\eta}$, where $\frac{d\hat{c}}{dr_d} < 0$ and $\frac{\partial Y}{\partial\eta} > 0$. Since $\frac{\partial Y}{\partial\hat{c}} = \eta^2\rho^2 + \eta\rho - \rho - \frac{2}{\alpha}\sigma$, substituting (40) yields $\frac{\partial Y}{\partial\hat{c}} = -(\rho^2 + \frac{2}{\alpha}\sigma\rho)\frac{1}{\hat{c}} < 0$. Thus we obtain $\frac{d\eta}{dr_d} < 0$.

With 1)-3), we complete the proof.

REFERENCES

[1] Z. Pi, and F. Khan, "An introduction to millimeter-wave mobile broadband systems," *IEEE Commun. Mag.*, vol. 49, no. 6, pp. 101-107, Jun. 2011.

[2] S. Rangan, T. S. Rappaport, and E. Erkip, "Millimeter-wave cellular wireless networks: Potentials and challenges," *Proc. of the IEEE*, vol. 102, no. 3, pp. 366-385, Mar. 2014.

[3] J. Brady, N. Behdad, and A. M. Sayeed, "Beamspace MIMO for millimeter-wave communications: System architecture, modeling, analysis, and measurements," *IEEE Trans. Antennas Propag.*, vol. 61, no. 7, pp. 3814-3827, Jul. 2013.

[4] M. R. Akdeniz, Y. Liu, M. K. Samimi, S. Sun, S. Rangan, T. S. Rappaport, and E. Erkip, "Millimeter wave channel modeling and cellular capacity evaluation," *IEEE J. Sel. Areas Commun.*, vol. 32, no. 6, pp. 1164-1179, Jun. 2014.

[5] A. Adhikary, E. Al Safadi, M. K. Samimi, R. Wang, G. Caire, T. S. Rappaport, and A. F. Molisch, "Joint spatial division and multiplexing for mm-wave channels," *IEEE J. Sel. Areas Commun.*, vol. 32, no. 6, pp. 1239-1255, Jun. 2014.

[6] O. El Ayach, S. Rajagopal, S. Abu-Surra, Z. Pi, and R. W. Heath, "Spatially sparse precoding in millimeter wave MIMO systems," *IEEE Trans. Wireless Commun.*, vol. 13, no. 3, pp. 1499-1513, Mar. 2014.

[7] Y. Lee, C. Wang, and Y. Huang, "A hybrid RF/Baseband precoding processor based on parallel-index-selection matrix-inversion-bypass simultaneous orthogonal matching pursuit for millimeter wave MIMO systems," *IEEE Trans. Signal Process.*, vol. 63, no. 2, pp. 305-317, Jan. 2015.

[8] A. Alkhateeb, O. El Ayach, G. Leus, and R. W. Heath, "Channel estimation and hybrid precoding for millimeter wave cellular systems," *IEEE J. Sel. Topics Signal Process.*, vol.8, no. 5, pp. 831-846, Oct. 2014.

[9] S. Hur, T. Kim, D. J. Love, J. V. Krogmeier, T. A. Thomas, and A. Ghosh, "Millimeter wave beamforming for wireless backhaul and access in small cell networks," *IEEE Trans. Commun.*, vol. 61, no. 10, pp. 4391-4403, Oct. 2013.

[10] T. Bai and R. W. Heath, "Coverage and rate analysis for millimeterwave cellular networks," *IEEE Trans. Wireless Commun.*, vol. 14, no. 2, pp. 1100-1114, Feb. 2015.

[11] S. Singh, M. N. Kulkarni, A. Ghosh, and J. G. Andrews, "Tractable model for rate in self-backhauled millimeter wave cellular networks," *IEEE J. Sel. Areas Commun.*, vol. 33, no. 10, pp. 2196-2211, Oct. 2015.

[12] A. D. Wyner, "The wire-tap channel," *Bell Syst. Tech. J.*, vol. 54, no. 8, pp. 1355-1387, Oct. 1975.

[13] N. Yang, L. Wang, G. Geraci, M. Elkashlan, J. Yuan, and M. Di Renzo, "Safeguarding 5G wireless communication networks using physical layer security," *IEEE Commun. Mag.*, vol. 53, no. 4, pp. 20-27, Apr. 2015.

[14] H.-M. Wang and X.-G. Xia, "Enhancing wireless secrecy via cooperation: signal design and optimization," *IEEE Commun. Mag.*, vol. 53, no. 12, pp. 47-53, Dec. 2015.

[15] A. Khisti, and G. W. Wornell, "Secure transmission with multiple antennas I: The MISOME wiretap channel," *IEEE Trans. Inf. Theory*, vol. 56, no. 7, pp. 3088-3104, Jul. 2010.

[16] H.-M. Wang, T.-X. Zheng, and X.-G. Xia, "Secure MISO wiretap channels with multi-antenna passive eavesdropper: artificial noise vs. artificial fast fading," *IEEE Trans. Wireless Commun.*, vol. 14, no. 1, pp. 94-106, Jan. 2015.

[17] S. Bashar, Z. Ding, and G. Y. Li, "On secrecy of codebook-based transmission beamforming under receiver limited feedback," *IEEE Trans. Wireless Commun.*, vol. 10, no. 4, pp. 1212-1223, Apr. 2011.

[18] H.-M. Wang, C. Wang, D. W. K. Ng, M. H. Lee, and J. Xiao, "Artificial noise assisted secure transmission for distributed antenna systems," *IEEE Trans. Signal Process.*, vol. 64. no. 15, pp. 4050-4064, Aug. 2016.

[19] X. Zhang, X. Zhou, and M. R. McKay, "On the design of artificial-noise-aided secure multi-antenna transmission in slow fading channels," *IEEE Trans. Veh. Technol.*, vol. 62, no. 5, pp. 2170-2181, Jun. 2013.

[20] N. Yang, P. L. Yeoh, M. Elkashlan, R. Schober and I. B. Collings, "Transmit Antenna Selection for Security Enhancement in MIMO Wiretap Channels," *IEEE Trans. Commun.*, vol. 61, no. 1, pp. 144-154, January 2013.

[21] X. Zhou, R. K. Ganti, and J. G. Andrews, "Secure wireless network connectivity with multi-antenna transmission," *IEEE Trans. Wireless Commun.*, vol. 10, no. 2, pp. 425-430, Feb. 2011.

[22] X. Zhang, X. Zhou, and M. R. McKay, "Enhancing secrecy with multi-antenna transmission in wireless ad hoc networks," *IEEE Trans. Inf. Forensics Security*, vol. 8, no. 11, pp. 1802-1814, Nov. 2013.

[23] H.-M. Wang, T.-X. Zheng, J. Yuan, D. Towsley, and M. H. Lee, "Physical layer security in heterogeneous cellular networks," *IEEE Trans. Commun.*, vol. 64, no. 3, pp. 1204-1219, Mar. 2016.

[24] H. Yin, D. Gesbert, M. Filippou, and Y. Liu, "A coordinated approach to channel estimation in large-scale multiple-antenna systems," *IEEE J. Sel. Areas Commun.*, vol. 31, no. 2, pp. 264-273, Feb. 2013.

[25] L. Wang, M. Elkashlan, T. Q. Duong, and R. W. Heath, "Secure communication in cellular networks: The benefits of millimeter wave mobile broadband," in *Proc. IEEE SPAWC*, Toronto, ON, Canada, Jun. 2014, pp. 115-119.

[26] N. Valliappan, A. Lozano, and R. W. Heath, "Antenna subset modulation for secure millimeter-wave wireless communication," *IEEE Trans. Commun.*, vol. 61, no. 8, pp. 3231-3245, Aug. 2013.

[27] N. Alotaibi, and K. Hamdi, "Switched phased-array transmission architecture for secure millimeter-wave wireless communication," *IEEE Trans. Commun.*, vol. 64, no. 3, pp. 1303-1312, Mar. 2016.

[28] M. E. Eltayeb; J. Choi; T. Y. Al-Naffouri; R. W. Heath, "Enhancing secrecy with multi-antenna transmission in millimeter wave vehicular communication systems," *IEEE Trans. Veh. Technol.*, vol. 66, no. 9, pp. 8139-8151, Sep. 2017.

[29] Y. Ramadan, H. Minn, and A. Ibrahim, "Hybrid analog-digital precoding design for secrecy mmWave MISO-OFDM systems," *IEEE Trans. Commun.*, 2017, doi:10.1109/TCOMM.2017.2734666.

[30] Y. Ju, H.-M. Wang, T.-X. Zheng and Q. Yin, "Secure transmissions in millimeter wave systems," *IEEE Trans. Commun.*, vol. 65, no. 5, pp. 2114-2127, May 2017.

[31] Y. Ju, H.-M. Wang, T.-X. Zheng, and Q. Yin, "Secure transmission with artificial noise in millimeter wave systems," in *Proc. IEEE WCNC*, Doha, Qatar, Apr. 2016, pp. 1-6.

[32] Y. Ju, H.-M. Wang, T.-X. Zheng, Y. Zhang, Q. Yang, and Q. Yin, "Secrecy throughput maximization for millimeter wave systems with artificial noise," in *Proc. IEEE PIMRC*, Valencia, Spain, Sep. 2016, pp. 1-6.

[33] C. Wang, and H.-M. Wang, "Physical layer security in millimeter wave cellular networks," *IEEE Trans. Wireless Commun.*, vol. 15, no. 8, pp. 5569-5585, Aug. 2016.

[34] S. Vuppala, S. Biswas, and T. Ratnarajah, "An analysis on secure communication in millimeter/micro-wave hybrid networks," *IEEE Trans. Commun.*, vol. 64, no. 8, pp. 3507-3519, Aug. 2016.

[35] Y. Zhu, L. Wang, K. K. Wong, and R. W. Heath, "Secure communications in millimeter wave ad hoc networks," *IEEE Trans. Wireless Commun.*, vol. 16, no. 5, pp. 3205?217, May 2017.

[36] C. Rusu, N. Gonzalez-Prelcic, and R. W. Heath, "An attack on antenna subset modulation for millimeter wave communication," in *Proc. IEEE ICASSP*, Brisbane, Australia, Apr. 2015, pp. 2914-2918.

[37] D. Tse, and P. Viswanath, *Fundamentals of Wireless Communication*. Cambridge, U. K.: Cambridge Univ. Press, 2005.

[38] A. M. Sayeed, "Deconstructing multiantenna fading channels," *IEEE Trans. Signal Process.*, vol. 50, no. 10, pp. 2563-2579, Oct. 2002.

[39] A. Ghosh, T. A. Thomas, M. C. Cudak, and R. Ratasuk, "Millimeter-wave enhanced local area systems: A high-data-rate approach for future wireless networks," *IEEE J. Sel. Areas Commun.*, vol. 32, no. 6, pp. 1152-1163, Jun. 2014.

[40] I. S. Gradshteyn, I. M. Ryzhik, A. Jeffrey, D. Zwillinger, and S. Technica, *Table of Integrals, Series, and Products*, 7th ed. New York: Academic Press, 2007.

[41] D. Stoyan, W. Kendall, and J. Mecke, *Stochastic Geometry and Its Applications*, 2nd ed. Hoboken, NJ, USA: Wiley, 1996.